1

Normal fault interactions in seismic cycles and the impact of fault network geometry

4

5 Constanza Rodriguez Piceda[1]*, Zoë K. Mildon[1], Martijn van den Ende[2], Jean-Paul Ampuero[2],
6 Billy J. Andrews[1]

7

8 *[1] University of Plymouth, School of Geography, Earth and Environmental Sciences, Plymouth, United*
9 *Kingdom*

10 *[2] Université Côte d'Azur, Observatoire de la Côte d'Azur, IRD, CNRS, Géoazur, Nice, France*

11

12 *Corresponding email: constanza.rodriguezpiceda@plymouth.ac.uk

Abstract

14 Understanding the mechanisms behind the characteristics of earthquake cycles on normal faults
15 is challenging due to their long recurrence times. Despite their moderate magnitude, normal
16 faulting earthquakes can produce considerable damage. We investigate the effects of fault
17 network geometry and spacing on the seismic cycle of a system of two normal faults modelled
18 with rate-and-state friction and elastic interactions. Our analysis examines how variable along-
19 strike and across-strike distances between faults influence cycle periodicity, synchronicity,
20 nucleation location, magnitude-frequency distribution, and rupture characteristics. To isolate
21 network-geometry effects from dimensional and frictional effects, we model faults with a
22 seismogenic width (W) over characteristic nucleation length (L_∞) ratio such that isolated faults
23 produce periodic cycles with a characteristic magnitude (Mw) of 5.1. The cycle periodicity and

24 Mw of earthquakes change depending on the spacing and geometry of the fault network. Faults

25 become less periodic at short across-strike distances (smaller than 0.2 km). Decreasing the

26 across-strike spacing leads to variable hypocenter locations and the emergence of partial

27 ruptures, producing magnitudes down to Mw 4.4 at spacings < 0.2 km. Cycle periodicity and

28 Mw remain unaffected by along-strike spacing. The long-term synchronization state of the

29 faults' seismic cycle is influenced differently by across-strike and along-strike distances.

30 Closely spaced faults (≤1.5 km) across-strike display fluctuating synchronization, whereas

31 faults arranged along-strike tend to evolve towards persistent synchronization as along-strike

32 separation decreases. Fault network geometry plays a prominent role, with across-strike

33 distance having a larger effect on interevent time and rupture style than along-strike distance.

34

Plain language summary

36 Normal faults generally produce earthquakes smaller than Mw 7 but can still cause significant

37 damage and loss of life. Understanding their seismic behavior is challenging due to these faults

38 having infrequent earthquakes, leading to limited geological and geophysical observations.

39 Physics-based models help bridge this gap by simulating multiple earthquakes, covering

40 multiple seismic cycles. In this study, we used high-performance computing to simulate

41 earthquakes on two normal faults, examining how their spatial arrangement and spacing

42 (across-strike vs. along-strike) affect their combined seismic cycle. We found the timing and

43 size of earthquakes depended on the faults' separation and arrangement. Widely separated

44 faults, regardless of their arrangement, show periodic earthquakes with equal magnitudes and

45 stable synchronization between faults over time. When faults are closer together across-strike,

46 earthquakes became less regular, and the synchronization between faults fluctuates.

47 Conversely, changing the along-strike spacing does not affect the periodicity or size of

48 earthquakes, but closer along-strike spacing led to more synchronized cycles. The separation

49 of faults across-strike has a greater impact on the characteristics of the earthquake cycle than

50 along-strike separation. We therefore expect the hazard posed by closely spaced across-strike

51 faults to be harder to forecast than those arranged along-strike from each other.

Key points

- Seismic cycles of faults far apart (>0.2 km) and across-strike are periodic, but become less periodic and out of phase when closer (<0.2 km).
- Seismic cycles on faults situated along-strike are periodic and, if initially asynchronized, become more synchronized over time when close together (<1 km).
- Across-strike distance impacts recurrence time, nucleation location, and magnitude-frequency distribution more than along-strike distance, which mainly affects fault synchronization.

Keywords: earthquake cycle, normal faults, fault interaction, recurrence time, synchronicity, rate-and-state friction

1. Introduction

The time interval between earthquakes on a same fault, also known as "recurrence time" or "interevent time", alongside the Coefficient of Variation of recurrence time (CV, the ratio of the standard deviation of recurrence time to their mean), are key inputs to model seismicity rates in probabilistic seismic hazard assessment (PSHA). In its classic form, PSHA is time-independent, which implies that earthquake occurrences are not influenced by previous seismic events or changes in stress states on faults (Cornell, 1968). This framework assumes that events of a similar magnitude rupture the same fault area in a quasi-periodic manner, thus faults should exhibit regular recurrence intervals (i.e., CV=0, Ellsworth, 1995). However, geological evidence suggests that this assumption may be an oversimplification and points towards the existence of periods of short interevent times alternating with periods of relative quiescence on a single fault (e.g., Kagan et al., 2012; Mildon et al., 2022; Mulargia et al., 2017). The time-dependent nature of earthquake recurrence intervals and related aperiodicity of the seismic cycle is a key source of uncertainty in PSHA (Gerstenberger et al., 2020). Most time-dependent hazard models utilize a single value of the CV, commonly derived from the paleoseismic record, to account for the changes in occurrence rate of earthquakes with time (e.g., Japan NSHM, Fujiwara et al., 2006; New Zealand NSHM, Stirling et al., 2012). Only few hazard

81 models have considered time-dependent processes like the occurrence of aftershocks and other

82 triggered events through the application of statistical models like the Epidemic Type

83 Aftershock Sequence or ETAS (e.g., UCERF3-ETAS in California, Field et al., 2017).

84 However, these are processes only considering short-term timescales (<50 years).

85 Evidence of the aperiodic character of the seismic cycle spanning timescales of 10^2-10^4 yr are

86 available from various geological and geophysical sources, including earthquake catalogues

87 (Frohlich & Davis, 1990; Kagan & Jackson, 1991; Reasenberg, 1985), slip histories (Benedetti

88 et al., 2013; Cowie et al., 2013; Goodall et al., 2021; Iezzi et al., 2021; Mildon et al., 2022),

89 and paleoseismic trenching (Cinti et al., 2021; Goldfinger et al., 2012; Marco et al., 1996;

90 McCalpin & Nishenko, 1996). The causative mechanisms behind the existence of aperiodic

91 seismic cycles are debated. Heterogeneous frictional properties along the fault plane (e.g.,

92 caused by localized occurrence of weak materials) has been shown to produce aperiodicity in

93 the earthquake cycle (e.g., Biemiller & Lavier, 2017; Dieterich & Richards-Dinger, 2010;

94 Hillers et al., 2007; Luo & Ampuero, 2018; Moore & Rymer, 2007).

95 An alternative explanation is that the stress on a fault can be altered due to stress interactions

96 with other faults within a fault network (Cowie et al., 2012, 2013; Marzocchi et al., 2009;

97 Mildon et al., 2017, 2019, 2022; Sgambato et al., 2020; Wedmore et al., 2017; Zöller & Hainzl,

98 2007). The concept is that an earthquake changes the surrounding stress field (Figure 1a-c),

99 stressing and advancing the occurrence of earthquakes on preferentially oriented faults, while

100 relaxing and delaying events on other faults. The regions where stress decreases after an

101 earthquakes are known as *stress shadows* (Harris & Simpson, 1996, 1998). The phenomena of

102 stress interaction between faults have been also discussed in the context of fracture mechanics

103 (Kachanov, 1987). The fault slipping zone can be represented as a *crack* and the interaction

104 between cracks may result in either a stress *amplification* (increase) or *shielding* (decrease)

105 depending on their geometrical configuration. In stacked configurations where cracks are

106 across-strike, a displacement on the tip on one crack causes a stress shielding effect in the

107 neighboring one. Conversely, collinear configurations where cracks are along-strike are

108 characterized by an *amplifying* effect of interaction: displacement on one crack produces an

109 increase of the stress field on the neighboring one (Kachanov et al. 1987). For both cases, the

110 magnitude of the stress interaction decreases with increasing distance between faults

111 (Kachanov et al. 1987).

112 Knowledge of the seismic cycles in natural fault systems is limited because of the incomplete
113 nature of the geological evidence (e.g., lack of fault exposures) and the relative short time
114 covered by earthquake and paleoseismic catalogs (e.g., Nicol et al., 2016). Physics-based
115 modelling of seismic cycles, including the coseismic, postseismic and interseismic phases
116 across numerous (>10) earthquake cycles, allows us to overcome some of these limitations.
117 Moreover, through these simulations, controlled experiments can be performed by manually
118 adjusting the characteristics of the fault, such as its area and frictional parameters, and
119 surrounding stress field. Previous numerical models have investigated the effects of fault
120 network geometry on the seismic cycle (e.g., Romanet et al., 2018; Yin et al., 2023). Early
121 studies focused on the effect of fault interaction by simulating a spring-block slider system
122 with two degrees of freedom (e.g. Abe & Kato, 2013; He, 2003; Yoshida & Kato, 2003). By
123 testing different friction parameters, complex fault slip behaviors, including seismic and
124 aseismic slip, and chaotic behavior were reproduced (Abe & Kato, 2013). Although these
125 models provided valuable insights on the seismic cycle, they assume the stability of the system
126 depends on a single critical stiffness, whereas faults in nature have multiple stiffnesses relevant
127 to the nucleation process (Rubin, 2008). Moreover, faults in these type of simulations cannot
128 produce partial ruptures, thus they likely underestimate the complexity of a seismic cycle
129 compared to a model with equivalent frictional properties but higher dimensionality (Li et al.,
130 2022). Therefore, higher-dimensional models are more suitable to explore the research question
131 of the effect of fault interaction in the seismic cycle. Romanet et al. (2018) modelled two 1D
132 partially overlapping strike-slip faults to study the effect of across-strike separation (among
133 other frictional parameters) on fault slip behavior. They identify that smaller distances between
134 faults can lead to the emergence of slow slip events and earthquake sequences with
135 spatiotemporal complexities. Yin et al. (2023) modelled a closer analog to a natural fault
136 system by simulating three 2D partially overlapping-strike slip faults with fixed across-strike
137 separation but varying frictional properties. They found that an isolated fault exhibits periodic
138 seismic cycles with full ruptures, whereas aperiodic stress patterns and partial ruptures emerge
139 when considering stress interactions within a fault network. While these studies unequivocally
140 show that complexities in the seismic cycle arises from fault interaction, it remains unclear how
141 these expressions of fault interaction might be influenced by the geometry of the fault network.
142 In this regard, geological observations from Italy suggest that the spatial arrangement of faults
143 across and along strike might impact the earthquake cycle of individual faults in the Apennines
144 (Sgambato et al., 2020, 2023). Areas with few faults arranged across-strike show relatively

5

145 periodic stress patterns (Figure 1e), while where multiple faults exist across-strike, the seismic
146 cycle of individual faults deviates from its characteristic behavior (Figure 1f).

147 With growing evidence highlighting the effect of fault interaction on seismic cycles, it becomes
148 increasingly relevant for the assessment of seismic hazard to better understand how the
149 geometry of fault networks influences seismic cycles on individual faults.
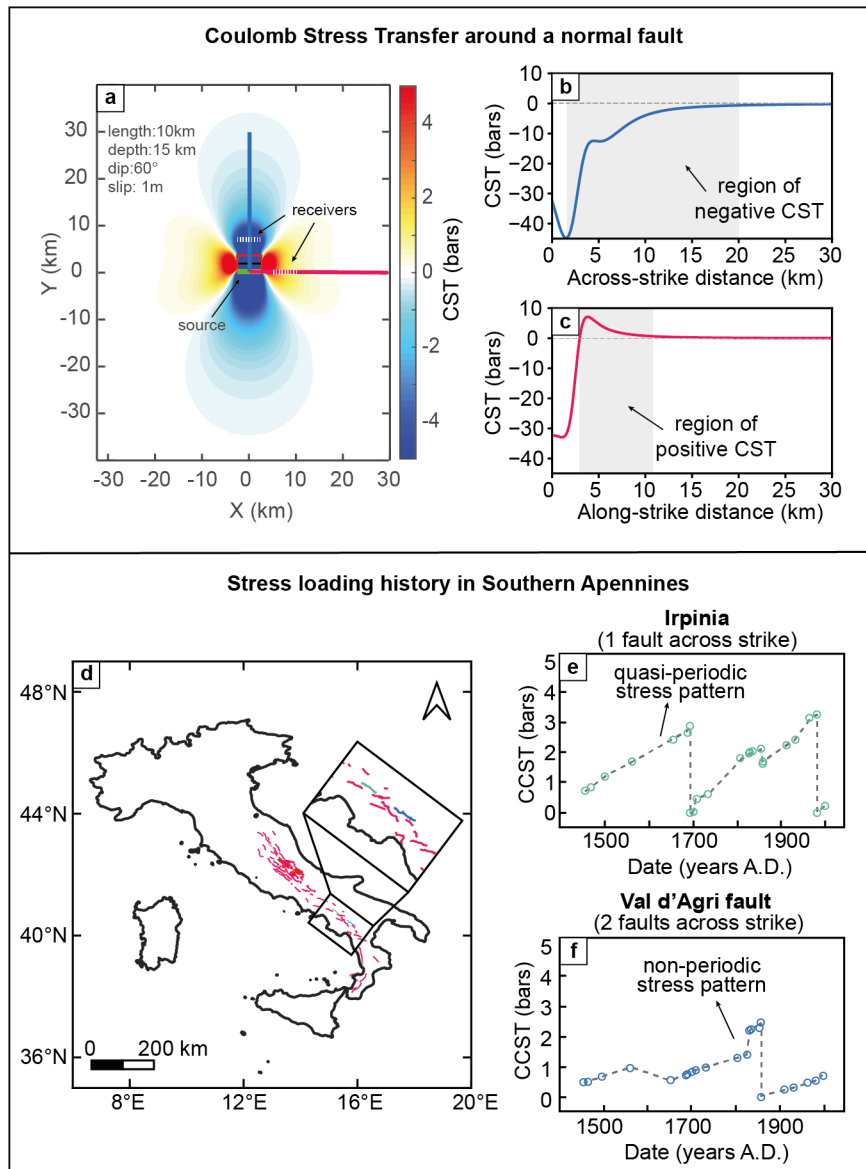
Figure 1. (a) Distribution of Coulomb stress transfer (CST) at 2.5 km depth induced by an earthquake in a 60° dipping normal fault (green line). Receiver faults situated across- and along-strike are depicted as dashed white lines. CST variation along two profiles **(b)** perpendicular and **(c)** parallel to

the fault, depicted in (a) by the blue and red lines, respectively. The grey-shaded area shows the distance range along which CST is negative or positive in (b) and (c), respectively. Note that this distance is larger in the across-strike profile, than in the along-strike profile. **(d)** Active fault traces in the central and southern Apennines, Italy, showing multiple faults across-strike for the central part and fewer normal faults across-strike for the southern part. Cumulative Coulomb stress transfer (CCST) time-series for a fault with: **(e)** 1 fault across strike, and **(f)** multiple faults across strike (modified from Sgambato et al., 2020). This example shows that relatively isolated faults have a simpler stress loading history than multiple faults arranged across-strike.

150 Previous numerical models of the earthquake cycle have primarily concentrated on strike-slip
151 fault systems due to geographic factors (such as heavily populated areas along the San Andreas
152 and North Anatolian faults) and computational advantages (Barbot, 2021; Dieterich &
153 Richards-Dinger, 2010; Robinson & Benites, 1995; Romanet et al., 2018; Ward, 2000; Yin et
154 al., 2023). Simulating a surface-breaking dip-slip fault introduces additional complexities as
155 normal stress changes must be computed due to the broken symmetry between hanging wall
156 and footwall relative to the Earth's free surface (Oglesby et al., 1998; Figure 2a). Additionally,
157 research targeting normal faults has been limited due to their lower seismicity rate and a
158 tendency to rarely exceed Mw>7 earthquakes (Wells & Coppersmith, 1994). However, normal
159 faults have the potential to generate events that can cause considerable damage and loss of life,
160 as evidenced by earthquakes like Mw 6.3 L'Aquila (Italy) in 2009, Mw 6.5 Norcia (Italy) in
161 2016, and Mw 7 Samos (Greece) in 2020.

162 In this study, we aim to answer the question *how does the fault network geometry impact the*
163 *seismic cycle of interacting normal faults?* To do that, we numerically simulate many seismic
164 cycles on two 2D normal faults embedded in a 3D medium and test how the along- and across-
165 strike spacing between them affects key parameters of the simulated earthquakes. In the
166 following sections, we use loosely the term "fault network", even though we model fewer faults
167 (two) than are typically found in natural fault systems. Our intention is to study essential
168 aspects of the process that can be captured by a pair of interacting faults. We examine three
169 key inputs for PSHA: interevent times within and between faults, magnitude-frequency
170 distributions, and nucleation locations. The latter might be a relevant parameter for the
171 estimation of point-source distances (Thompson & Worden, 2017) and to consider rupture
172 directivity effects in PSHA models (Spagnuolo et al., 2012). Our key finding is that these three
173 inputs, alongside the seismic rupture style, exhibit a consistent variation with changing distance

174 between faults. Moreover, the geometry of the fault network plays a prominent role, with
175 across-strike separation between faults producing more spatiotemporal complexities than
176 along-strike distance.

177

2. Methods

179 We performed multicycle simulations of two 2D planar normal faults embedded in a 3D elastic
180 medium using the boundary-element method code QDYN (Luo et al., 2017). This code
181 considers that the fault is infinite, but only applies friction conditions on a finite-length segment
182 of each fault. Beyond this segment, a constant slip velocity is prescribed.

183 2.1. Governing equations

184 Fault friction in our model evolves following the classical rate-and-state friction law (Dieterich,
185 1979; Marone, 1998; Ruina, 1983). This law considers that the fault is non-stationary, thus the
186 shear stress (τ) along the fault is equal to its frictional strength:

$$\tau = \mu\sigma \quad (1)$$

188 where μ is the friction coefficient and σ is the effective normal stress (total normal stress minus
189 pore-fluid pressure). Friction $\mu(V,\theta)$ depends on the slip rate (V) and a state variable (θ):

$$\mu(\theta, V) = \mu_0 + a\,\ln\left(\frac{V}{V_0}\right) + b\ln\left(\frac{V_0\theta}{D_c}\right) \quad (2)$$

191 where μ_0 is the reference friction coefficient measured at a reference slip rate V_0; a and b are
192 constants that quantify the instantaneous effect of V and evolution effect of θ on μ,
193 respectively; D_c is the characteristic slip distance over which the fault evolves towards a new
194 steady state. The state variable θ evolves following the ageing law (Eq. 3, Dieterich, 1979;
195 Ruina, 1983):

$$\frac{d\theta}{dt} = 1 - \frac{V\theta}{D_c} \quad (3)$$

197 In steady-state, $\frac{d\theta}{dt} = 0$, thus steady-state friction μ_{ss} is:

198
$$\mu_{ss} = \mu_0 + (a-b)ln\frac{V}{V_0} \quad (4)$$

199   The term (a-b) quantifies the velocity-dependence of μ at steady-state. When (a-b) > 0, the
200   material is velocity-strengthening, meaning that friction increases with increasing slip rate. In
201   this regime, sliding is stable. When (a-b) < 0, the material is velocity-weakening, where friction
202   decreases as slip rate increases. Velocity-weakening faults are conditionally stable: they
203   produce unstable sliding if their length L exceeds a so-called limiting value of the nucleation
204   length (L_∞) (Rubin and Ampuero, 2005):

205
$$L_\infty = \frac{1}{\pi}\left(\frac{b}{b-a}\right)^2 \frac{GD_c}{b\sigma} \quad (5)$$

206   where G is the shear modulus, and aseismic behavior otherwise (Rubin & Ampuero, 2005),
207   unless subject to large enough perturbations (Gu & Wong, 1994).

208   QDYN solves the equation of elastostatic equilibrium under a quasi-dynamic approximation,
209   which relates the stress and the slip rate on a point of a fault (Rice, 1993):

210
$$\tau_0 + \tau_e - \frac{G}{2c}V = \sigma\mu \quad (6)$$

211   where τ_0 is the initial shear stress, τ_e is the elastic shear stress change induced by slip, σ is the
212   effective normal stress emerging from the initial condition and the fault interaction, and $\frac{G}{2c}V$ is
213   the radiation damping term, which approximates the effects of stress change due to wave
214   propagation during sliding. c the shear-wave speed.

215   When the slip rate of a fault element differs from the tectonic slip rate V_{PL}, it transmits stresses
216   to the other fault elements. The elastic shear stress in a fault cell τ_i^e is the sum of the shear
217   stress at the i-th fault cell resulting from the slip on all fault cells, and is expressed as:

218
$$\tau_i^e = -\sum_j k_{ij}^\tau\big(u_j(t) - V_{PL}t\big) \quad (7)$$

219   where u_j is the slip on the j-th cell and k_{ij}^τ is the stiffness matrix for shear stress, which contains
220   the shear stress change on the i-th fault element induced by a unit slip on the j-th fault element.
221   The stiffness matrix is computed using the analytical formulations of Okada (1992) for static

222   stresses induced by rectangular dislocations. The normal stress σ is the sum of the initial normal

223   stress σ_0 and the elastic normal stress (σ_e):

224    $$\sigma = \sigma_0 + \sigma_e \qquad (8)$$

225   The calculation of elastic normal stress follows a similar form to that of Eq. 7 but involves the

226   stiffness matrix for normal stress k_{ij}^{σ}:

227

228    $$\sigma_i^e = -\sum_j k_{ij}^{\sigma}\big(u_j(t) - V_{PL}t\big) \qquad (9)$$

229

230   ## 2.2 Model set up

231   We modeled two 2D parallel normal faults of 60° dip with equal dimensions and distribution

232   of frictional properties (Table 1). We tested a setup of two small faults of 5 km length and 3

233   km width (Figure 2b-c), extending from 3 to 6 km depth. Despite their smaller size in

234   comparison to natural faults causing damaging earthquakes, we opted for these dimensions to

235   ensure that modelling of individual faults yields relatively similar seismic events (i.e., few

236   partial ruptures). Additionally, the faults were initiated with equal stress conditions. These

237   choices enabled us to focus on our key question of how fault spacing affects earthquake

238   occurrence. The faults consisted of a rectangular area of velocity weakening properties (i.e.,

239   asperity or seismogenic patch) surrounded by a 500-m wide area of velocity-strengthening

240   material introduced to smooth out the transition to the steadily creeping fault areas.

241   The length scale setting the minimum mesh size needed to properly resolve the nucleation and

242   propagation of rupture is the process or cohesive zone length (L_b):

243    $$L_b = \frac{GD_c}{b\sigma} \qquad (10)$$

244   The element size (Δx and Δw) needs to be set at least three times smaller than L_b (Day et al.,

245   2005). We choose $L_b/\Delta x \sim 5$ and $L_b/\Delta w \sim 4$ to ensure adequate resolution of the process zone,

246   while keeping a feasible computation time.

247   The overall behavior of slip on a fault is controlled by the ratio of its shortest edge length (W_s)

248   to the nucleation length (L_∞, Rubin & Ampuero, 2005; Eq. 5). Faults can produce irregular

249   cycles including both fully and partial ruptures if W_s/L_∞ is high, while a W_s/L_∞ ratio

250   moderately larger than 1 leads to regular characteristic cycles with only full ruptures (Barbot,

251   2019; Cattania, 2019; Cattania & Segall, 2019). The exact value of W_s/L_∞ above which

252   complex seismicity is generated seems to depend on the simulation dimensionality and the

253   shape of the asperity. For 1D faults, partial ruptures emerge with a W_s/L_∞ ratio higher than 10

254   (Cattania, 2019). For 2D faults with a circular seismogenic patch, increasing complexity arises

255   by increasing the ratio between the radius of the asperity and nucleation length (Cattania &

256   Segall, 2019). These authors found that partial ruptures emerge with a ratio of 29.6. Following

257   these studies, we set the W_s/L_∞ ratio to be 10.2, to ensure that single faults generate mostly full

258   ruptures.

259   To avoid effects related to unrealistic symmetries imposed by uniform fault properties, while

260   keeping the faults relatively similar, we introduce random Perlin noise (i.e. a type of random-

261   looking but coherent noise pattern, Perlin, 1985) with 0.1% variation in the values of b. Both

262   faults display a different noise distribution. We tested a broad range (0.05 – 1000 km) of across-

263   and along-strike spacing, bringing the total number of simulations to 43 (Table 1). Although

264   faults spaced 100 or 1000 km apart are not typically considered part of the same fault network

265   in natural systems with equivalent fault dimensions, we included these spacings to represent

266   cases of isolated faults. "Spacing" here refers to the closest spacing between fault tips. If we

267   were to measure along-strike distance as the spacing between centers of the faults, an additional

268   5 km should be considered. By this latter definition, if the along-strike distance were less than

269   5 km, the faults would be superposed, which is a scenario that cannot be modelled and is not

270   realistic in the natural world. One approximation of such scenario would be to model a single

271   fault consisting of two asperities with the same size as the individual faults separated by a

272   varying-sized velocity-strengthening barrier. However, since this scenario has been extensively

273   studied in existing literature (Corbi et al., 2017; Kaneko et al., 2010; Molina-Ormazabal et al.,

274   2023; Wei & Shi, 2021), we opt not to model it. Consequently, our study extends previous

275   work on asperity interactions, focusing on cases with an asperity spacing that tends to infinity.

276   We ran the simulations for 2000 yrs and we discarded the initial warm-up cycles during the

277   first 100 yrs (~3 cycles).

278

279   **Table 1:** Model set-up describing material and frictional properties, fault geometry and spatial offsets
280   between faults. VW= velocity weakening region, VS= velocity-strengthening region; *following
281   Lapusta et al. (2000) and accounting for the dip angle (60°, see Supplementary Text 1).

Symbol	Description (units)	Value
Material properties		
G	Shear modulus (Pa)	3e10
λ	Elastic modulus (Pa)	3e10
c	Shear wave velocity (m/s)	3000
Frictional properties		
μ*	Reference friction coefficient	0.6
a	Direct-effect parameter	0.007
b	Evolution effect parameter	0.014 (VW) / 0.0042 (VS)
D_c	Characteristic slip distance (m)	2e-3
V_{PL}	loading rate (m/s)	1e-10 (3.15 mm/yr)
V*	Reference slip rate (m/s)	1e-9
σ	Initial effective normal stress (Pa)	43.3e6*
Lb	Process zone width (m)	98

		$\dfrac{G.Dc}{b.\sigma}$	
L_∞	Limiting nucleation length value (m) $\dfrac{1}{\pi}\left(\dfrac{b}{b-a}\right)^2 L_b$	196	
Geometry			
Lf	Fault segment length (km)	5	
Wf	Fault segment width (km)	3	
L	Velocity-weakening length (km)	4	
W	Velocity-weakening width (km)	2	
Δx	Along-strike element size (m)	19	
Δw	Along-width element size (m)	24	
N	Number of individual fault elements	31232	
Nx	Number of fault elements along strike	256	
Nw	Number of fault elements across strike	122	
Ratio L_b/Δx (L_b/Δw)	Ratio for mesh resolution	5 (4)	
Z_corner	Depth of fault bottom (km b.m.s.l.)	6	

dy	Across-strike spacing (km)	0.1, 0.2, 0.3, 0.4, 0.5, 0.6, 0.7, 0.8, 0.9, 1, 1.5, 2, 2.5, 3, 5, 10, 100, 1000
dx	Along-strike spacing (km)	0.05, 0.1, 0.2, 0.3, 0.4, 0.5, 0.6, 0.7, 0.8, 0.9, 1, 1.2, 1.5, 2, 2.5, 3, 5, 10, 100

282

283
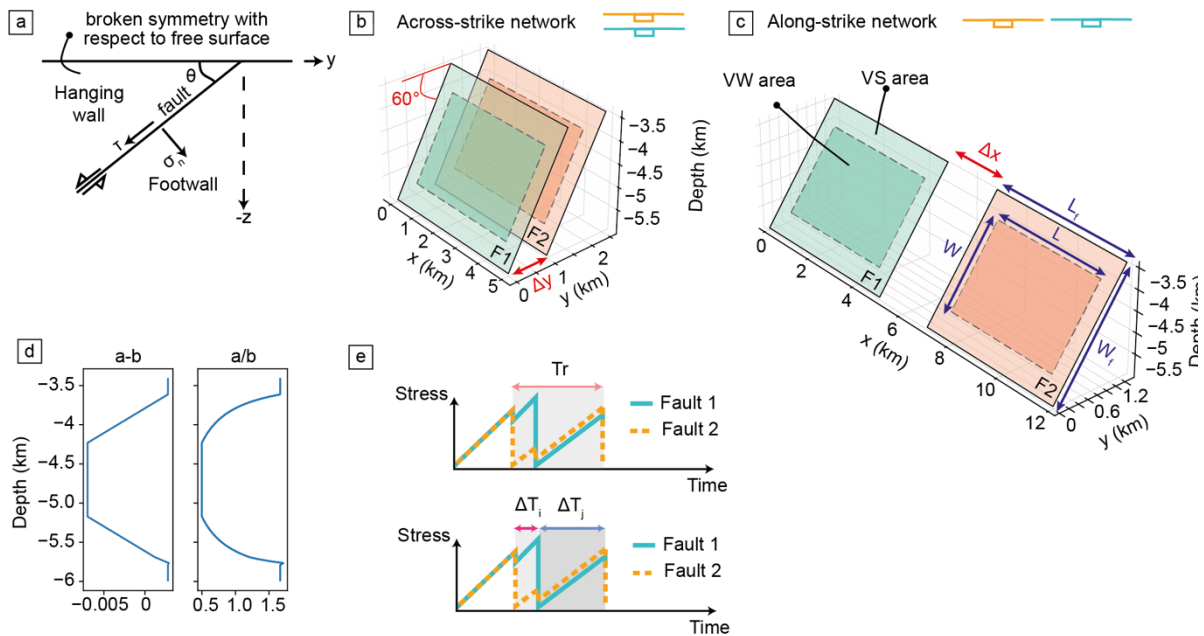
Figure 2: (a) Schematic diagram of a normal fault showing the broken symmetry of the two sides of the fault with respect to the free surface (modified from Oglesby et al., 1998). 3D visualization of the model set-up for the network of **(b)** across-strike faults and of **(c)** along-strike faults. The area with darker colors is velocity-weakening (VW), while the area with lighter colors is velocity-strengthening (VS). **(d)** Depth profiles showing the distribution of frictional parameters a and b. **(e)** Schematic diagrams of stress-loading history of two faults showing recurrence time (Tr) for fault 2 and time difference between the previous and the next event on the other fault (ΔT_i, ΔT_j).

284

3. Results

3.1 Periodicity and synchronicity of seismic cycles

To analyze the effect of the fault spacing on the periodicity of earthquakes on a fault and a fault system, we use two key metrics: the recurrence time of events, defined as the time interval between consecutive events on the same fault (T_r, Figure 2e) and the coefficient of variation of the recurrence times on the fault (CV) defined by $CV = \frac{std(T_r)}{mean(T_r)}$. If CV = 0, seismic events are periodic; if CV = 1, earthquakes follow a Poissonian distribution, independent of one another; if CV > 1, events are clustered (Boschi et al., 1995). An event is defined as ongoing if at least one fault element is slipping with a velocity larger than 0.01 m/s.
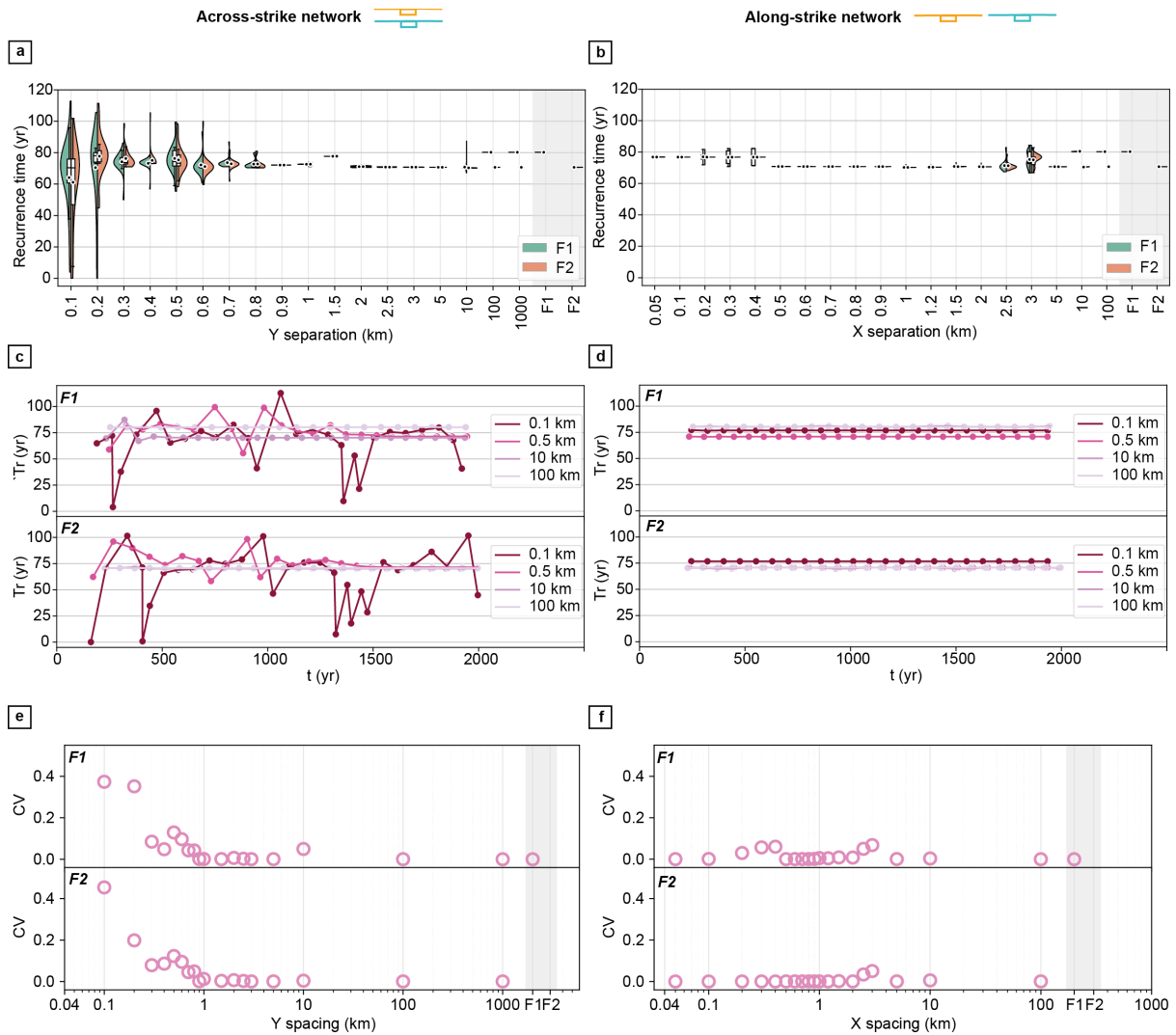
Figure 3. (a-b) Variation of recurrence time (Tr) of individual faults (shown as kernel density estimation and boxplot) as a function of the **(a)** across-strike and **(b)** along-strike spacing between faults. **(c-d)** Time-series of the recurrence time of individual faults for selected **(c)** across-strike and **(d)** along-strike spacings (0.1, 0.5, 10 and 100 km). **(e-f)** Variation of CV on individual faults as a function of the spacing between faults. Panels (e) and (f) correspond to the across- and along-strike system, respectively. CV depends on fault separation for faults that are across-strike, with greater CV values when the faults are closer. There is no similar CV dependence for the models with faults that are along-strike.

The periodicity and recurrence time are influenced by the across-strike distance between faults (Figure 3). Seismicity on isolated faults is almost periodic, as shown by CV values close to 0 (F1 and F2 in Figure 3e-f), and have recurrence times of 80 and 70 years in Fault 1 and Fault 2 (Figure 3a-b). As expected, in simulations where faults have large across-strike spacing (>10 km), the recurrence time distribution and CV are similar to those of the isolated faults (Figure 3a,c,e). As the across-strike distance decreases (0.8-10 km), models show regular recurrence times for individual faults, with values that may either match or differ from those observed in isolated faults albeit with values different than those of isolated faults (all model groups; Figure 3a). With decreasing across-strike distance (<0.8 km), faults show a wider range of recurrence times, regardless of the frictional distribution of the faults, with some as small as ~3 years (Figure 3a). When the across-strike distance between faults is <0.2 km, the range is even larger and faults show recurrence times > 100 years and become less periodic (CV~0.2-0.45; Figure 3a,c,e). The largest variability of recurrence time (CV~0.5) occurs when the across-strike spacing is the smallest (0.1 km, Figure 3a,c,e).

Contrastingly, in the along-strike system, both distant and nearby faults have recurrence times of ~70 or 80 years with little variability, as depicted by the distributions of the individual faults and the CV~0 for most along-strike distances in all model groups (Figure 3b,d,f). For separations down to 0.5 km, Tr is equal to the smaller of the two values, while for separations smaller than 0.5 km, Tr lies between the two values (Figure 3b,d).

In the following, we examine how the synchronization of the seismic cycles of the two faults varies with fault spacing (Figure 4). We compute two measures: the synchronicity coefficient S and the phase delay ϕ. S is defined as:

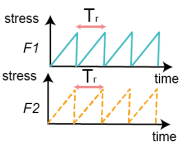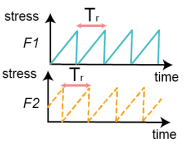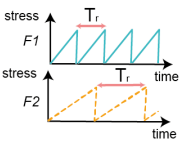$$S = \frac{|\overline{Tr_{F1}} - \overline{Tr_{F2}}|}{\frac{\overline{Tr_{F1}} + \overline{Tr_{F2}}}{2}} \quad (11)$$
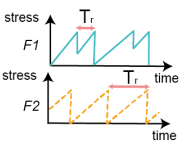
where $\overline{Tr_{F1}}$ and $\overline{Tr_{F2}}$ are the average recurrence times of Fault 1 and Fault 2, respectively, during the entire model run. S ranges from 0 to 1, with S=0 denoting that the recurrence times are equal, while S=1 indicating that the average recurrence times of the two faults are different. The phase delay ϕ over time is calculated as:

$$\phi = \frac{2\min(\Delta T_i - \Delta T_j)}{\frac{Tr_{F1} + \overline{Tr_{F2}}}{2}} \quad (12)$$

Where ΔT_i and ΔT_j is the time difference between the preceding and the following event on the other fault, respectively (Figure 2e). ϕ is computed for each earthquake within the catalogue. This allows us to study both if synchronicity evolves over time and how the average synchronization varies with fault spacing. Despite having different recurrence times, the faults of the model groups tested so far were initialized with the same stress conditions. To analyze the effect of fault spacing in the synchronization between faults with different initial stresses, we ran a variation of the models where faults 1 and 2 were initiated with stress states corresponding to the co-seismic and the inter-seismic stage of their seismic cycle, respectively. Overall, we aim to interpret broad trends of how synchronization depends on fault spacing. The synchronization between the combined cycles of two faults can take the following forms (Figure 4):

1) *In-phase synchronization*: if the recurrence times of both faults are the same (S~0) and there is no phase delay ($\phi = 0$), the seismic cycles of two faults will be perfectly synchronized.

2) *Out-of-phase synchronization:* if the recurrence times of both faults are the same (S~0), and ϕ is constant and larger than 0, the seismic cycles will be synchronized in terms of recurrence but offset in time.

3) *Oscillatory synchronization:* when faults are initialized with the same stressing conditions but have constant and different recurrence times, S ≠0 and ϕ will show a periodic oscillation, indicating more and less in-phase cycles; e.g. if fault 1 has a recurrence time of 70 years, fault 2 has a recurrence time of 80 years, the faults will appear to be in phase at 560 years, but then will gradually become out of phase.

354　　4) *Asynchronized:* when the recurrence times of the two faults are different and ϕ varies

355　　　　over time, the seismic events on the faults will not align regularly.

| Seismic cycle	Synchronicity coefficient (S)	Phase delay (Φ)	Synchronization state
	S=0	Φ = 0	in-phase synchronization
	S=0	constant Φ>0	out-of-phase synchronization
	S≠0	Φ with periodic oscilation	oscillating synchronization over time
	S=1	Φ variable over time	asynchonization

356

357　　**Figure 4**: Schematic diagrams showing the possible synchronization states of the seismic

358　　cycles of two faults.

359　　When the faults are sufficiently far apart so there is no interaction, they are expected to exhibit

360　　oscillatory synchronization with periodic shifts in phase delay (Figures 5 and 6). However,

361　　when the faults are close enough to interact, this behavior is expected to evolve throughout the

362　　simulation. The long-term synchronicity behavior between fault seismic cycles is affected by

363　　across-strike and along-strike distances differently (Figures 5, 6, S1). In the across-strike

364　　system, closely spaced faults (<= 10 km) display a different trend compared to those further

365　　apart: for spacings between 1km and 10 km, the cycle of the two faults is synchronized (S~0,

366　　Figure 5a, 6a) and out of phase, with constant phase delay between cycles (Figure 5c, 6c, S1a);

367　　for spacings further smaller spacings, S~0 (Figure 5a, 6a), but the phase delay fluctuates over

368　　time with alternating, non-periodic, intervals of higher and lower phase delay, meaning that the

369　　seismic cycles of the two faults are asynchronized (Figure 5c; 6c; S1a). Contrastingly, in the

370　　along-strike network, with decreasing spacing (< 10 km) faults with equal initial stress

371　　conditions tend to evolve from a state of out-of-phase synchronization (S=0, Figure 5b; ϕ>0,

372　　Figure 6b, S1b) to a state of in-phase synchronization (S=0, Figure 5b; ϕ = 0). Interestingly,

373　　faults with different stressing conditions also become more synchronized behave similarly to

374   those with equal initial stressing conditions, but with spacings < 0.2 km, they become slightly

375   out-of phase ($\phi = 0$, Figure 6b).

376   To summarize, our results indicate that fault geometry (i.e., the across- and along-strike

377   separation between faults) affects the recurrence intervals, CV and synchronicity of

378   earthquakes. For across-strike faults, when the faults are close together, the recurrence times

379   and synchronization are highly variable indicating faults are rupturing at different times with

380   no periodic behavior. When across-strike faults are far apart, the recurrence times are more

381   consistent and the phase delay between seismic cycles is oscillatory. Conversely for along-

382   strike faults, faults with different recurrence time tend to converge to the same value, with CV

383   close to zero indicating periodic behavior. Finally, as along-strike distance decreases, the

384   combined seismic cycle of faults with different initial stress conditions transitions towards an

385   in-phase synchronization state, resulting in co-rupture at short distances.
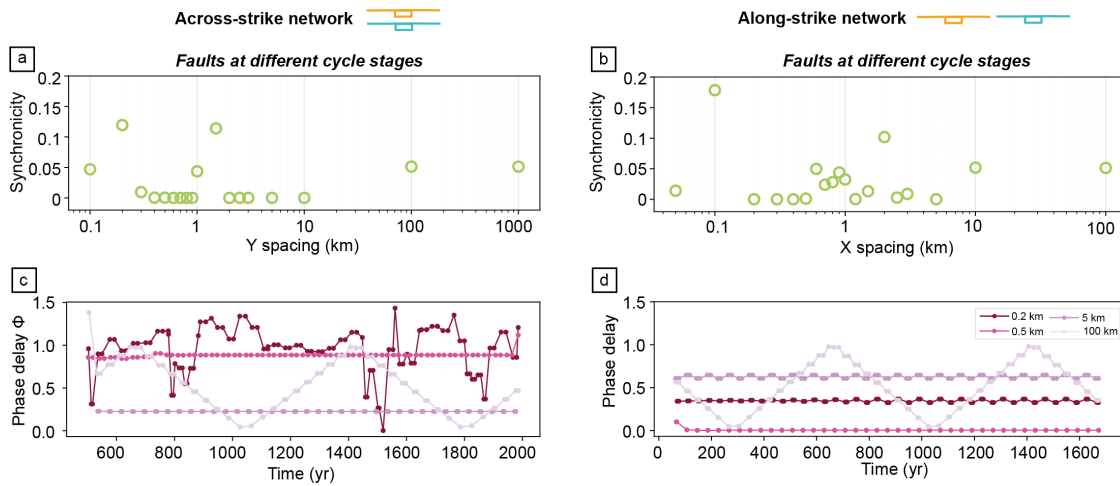
386
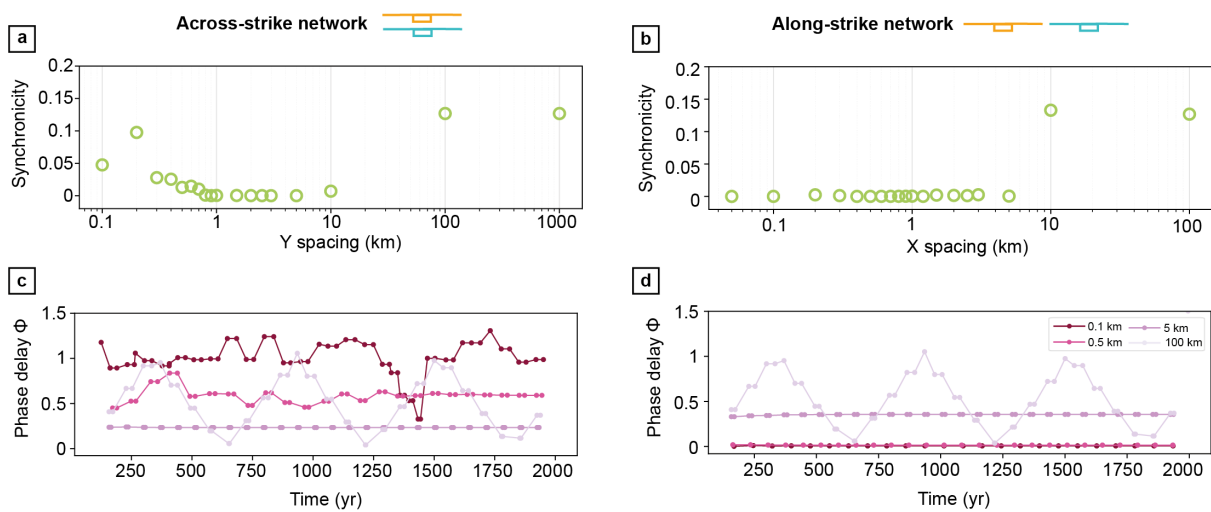
387

388   **Figure 5.** Synchronicity for the model group where individual faults are initialized at the same stage of

389   the seismic cycle. **(a-b)** Variation of the synchronicity with increasing separation for the **(a)** across-

390   strike and **(b)** along-strike system for all model groups. **(c-d)** Variation of phase delay ϕ with time for

391   specific fault separations (0.1, 0.5, 5 and 100 km; color legend is depicted in (b)) for the **(a,c)** across-

392   strike and **(b,d)** along-strike systems. The seismic cycles of across-strike faults display variable degrees

393   of synchronization as separation distance decreases, while cycles of along-strike faults turn consistently

394   more in-phase with decreasing distance (<=0.9 km).

395

Figure 6. Synchronicity for the model group where individual faults are initialized at different stages of the seismic cycle. **(a-b)** Variation of the synchronicity with increasing separation for the **(c)** across-strike and **(d)** along-strike networks. **(d-c)** Variation of phase delay φ with time for specific fault separations (0.1, 0.5, 5 and 100 km) for the **(d)** across-strike and **(c)** along-strike networks.

To summarize, our results indicate that fault geometry (i.e., the across- and along-strike separation between faults) affects the recurrence intervals, CV and synchronicity of earthquakes. For across-strike faults, when the faults are close together, the recurrence times and synchronization are highly variable, and the synchronization is relatively low indicating faults are rupturing at different times. When across-strike faults are far apart, the recurrence times are more consistent and the synchronization is greater. Conversely for along-strike faults, the recurrence time is mostly independent of along-strike distance between the faults, with CV close to zero indicating periodic behavior. Finally, as along-strike distance decreases, the combined seismic cycle of faults with different initial stress conditions transitions towards a persistent synchronization state, resulting in co-rupture at short distances.

20

3.2. Magnitude-frequency distribution
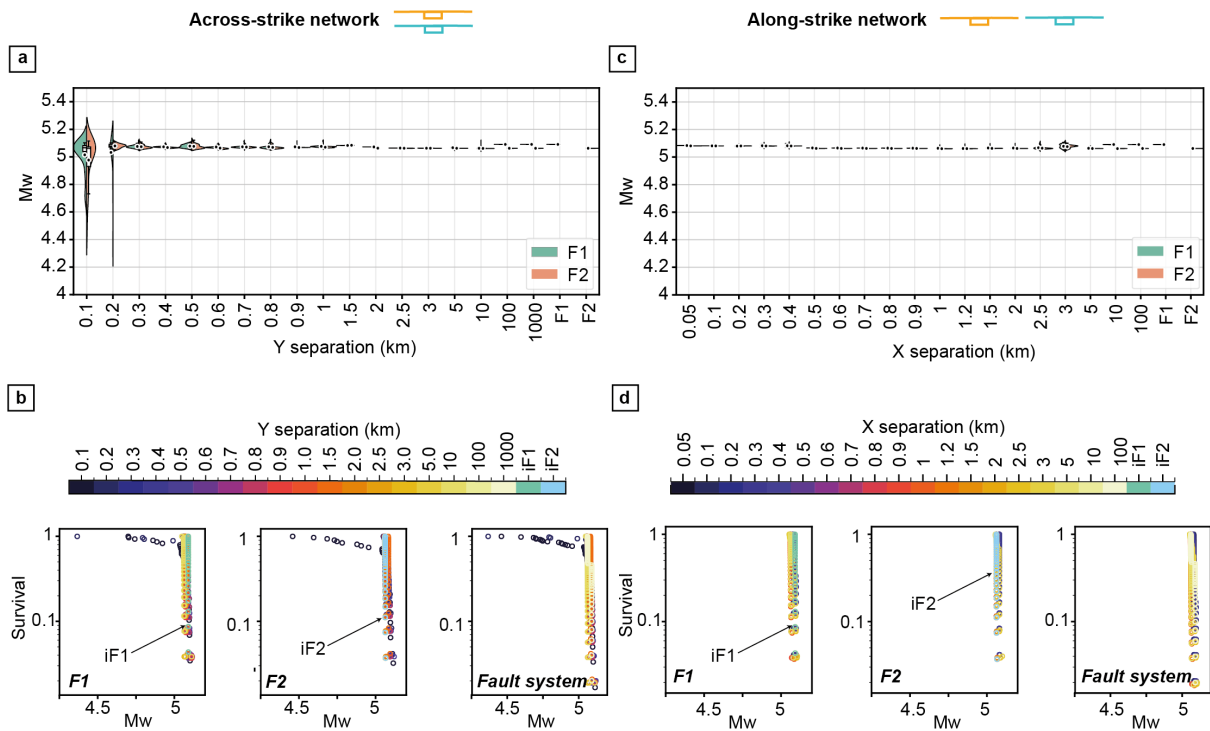
Figure 7. Magnitude-frequency distributions of events for different fault separations. Panels a-b and c-d belong to the across- and along-strike network respectively. Panels a and c correspond to the histograms of Mw (shown as kernel density estimation and boxplot) of individual faults, while panels b and d show the survival function (defined as the number of events with magnitude larger than a certain Mw, normalized by the total number of events in the fault) color-coded by the spacing between faults. Left, middle and right subpanels correspond to Fault 1, Fault 2 and the fault system, respectively. The general trend is that there is a greater range in the frequency-magnitude distribution for the across-strike fault network than for the along-strike fault network.

We analyze the effect of changing spacing between faults on the earthquake magnitude-frequency distribution. The shape of distributions differs for the across- and along-strike fault networks (Figure 8). In the across-strike network, faults with spacing >0.2 km show a characteristic magnitude Mw 5.1, while faults with decreasing spacing display a skewed distribution featuring an increasing number of smaller events with a lower limit of magnitudes of Mw 4.4 (Figure 8a-b). In the along-strike fault network, faults showed a characteristic-earthquake behavior with magnitude of Mw 5.1 irrespective of spacing (Figure 8c-d). In summary, changing fault separation affects the earthquake magnitude distribution only in cases of small across-strike spacing.

430 3.3. Nucleation and propagation of seismic events
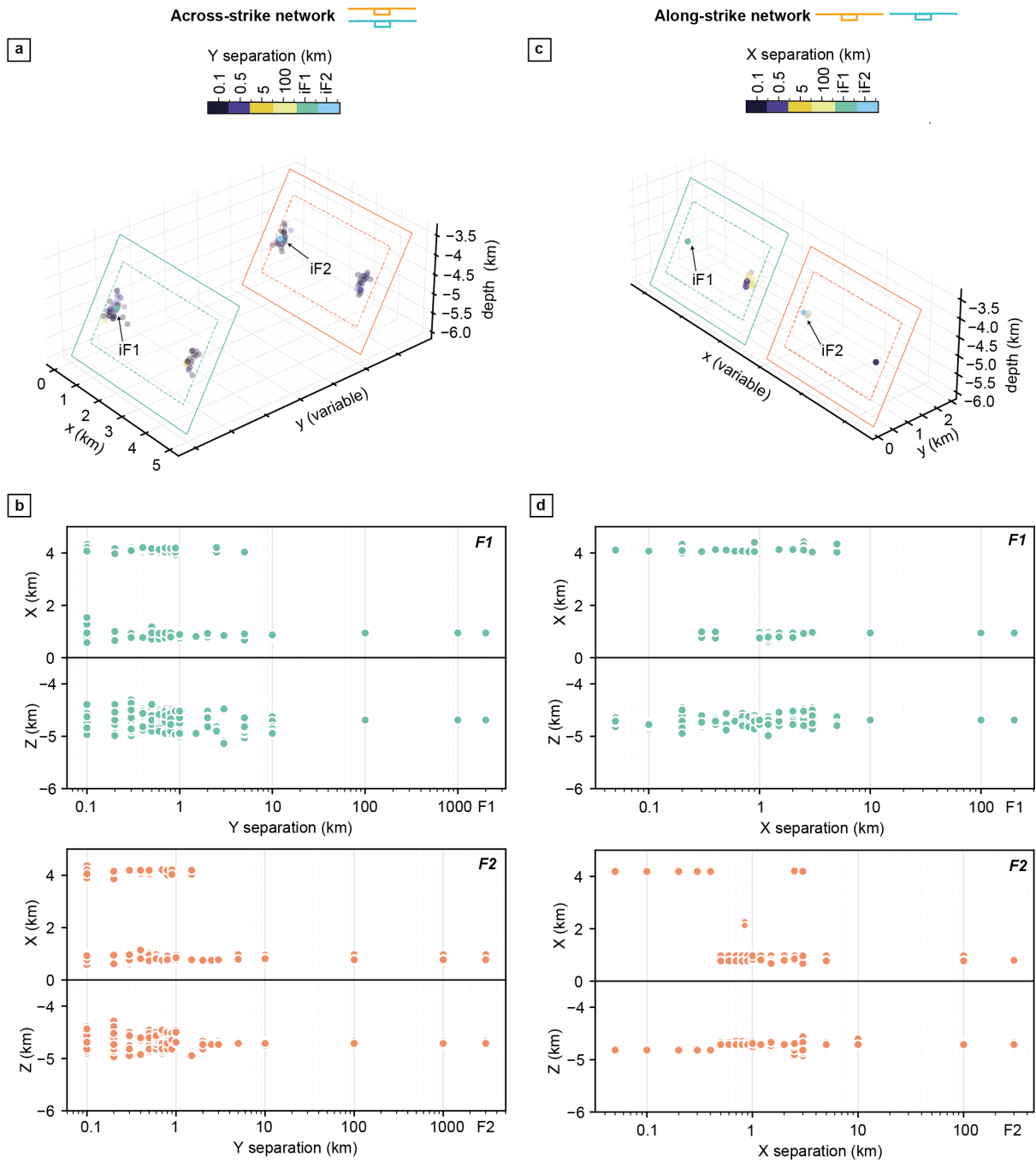
Figure 8. (a,c) Location of nucleation point color-coded by selected fault spacings. The spacing of faults displayed in the panels a and c is fixed for visualization purposes even though a range of spacing values is considered. **(b,d)** X and Z coordinates of nucleation points of individual faults for all modelled fault spacings. Panels a and b correspond to the across-strike network, and panels c and d to the along-strike network. For models with isolated faults (iF1 and iF2, blue and green dots in panels a and c), nucleation locations are consistently near one lateral edge of the fault. In contrast, for all models with

438   two faults, the nucleation locations are more spatially distributed and vary with fault spacing and from
439   one cycle to the next.

440   We analyze the effect of the spacing between faults on the nucleation and propagation of
441   events. For isolated faults, events initiate on the middle-left edge of the asperity (region of
442   velocity-weakening material). In the across-strike network, nucleation of events appears to be
443   more evenly distributed along both right and left edges (Figure 8a-b). Moreover, these events
444   nucleate both above and below the central part of the fault. Notably, for across-strike distances
445   < 1 km, few seismic events nucleate towards the center of the asperity (Figure 8a). In the along-
446   strike network, while most events nucleate on the left side of the faults, the nucleation on the
447   right side of the fault starts to emerge when the along-strike spacing is less than or equal to 5
448   km (Figure 8c-d).
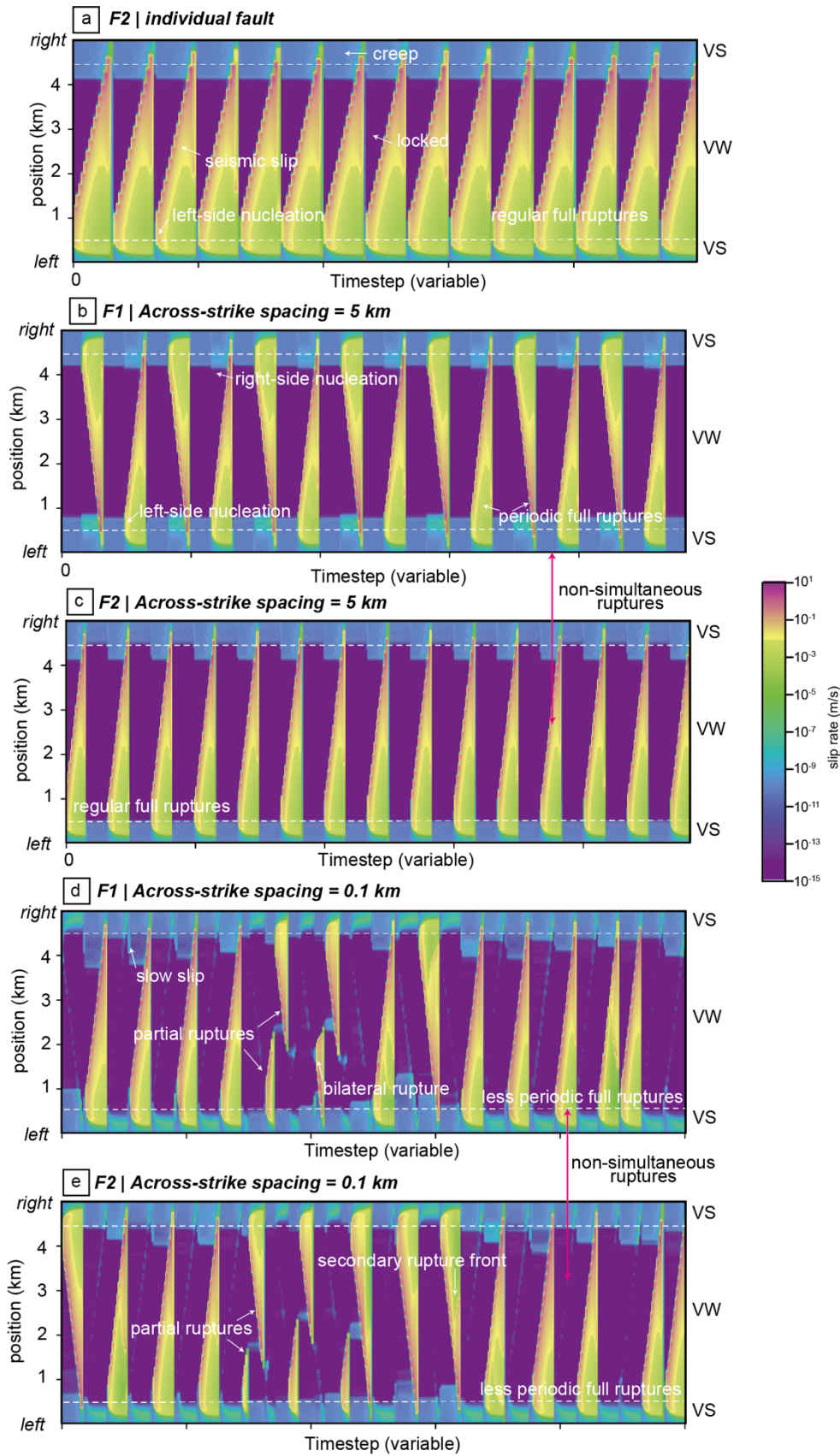
Figure 9: Evolution of the slip rate along a horizontal profile taken at the middle of the fault for a) the individual fault 2, and both faults at across-strike distances of b-c) 5 km and d-e) 0.1 km during the last

452   1000 years of the simulation. The plots show the increasing complexity in the rupture front of the fault

453   with decreasing across-strike spacing. Note that, due to QDYN's adaptive time-stepping, in the co-

454   seismic period timesteps are smaller than in the inter-seismic period. VS = velocity strengthening, VW

455   = velocity weakening.

456
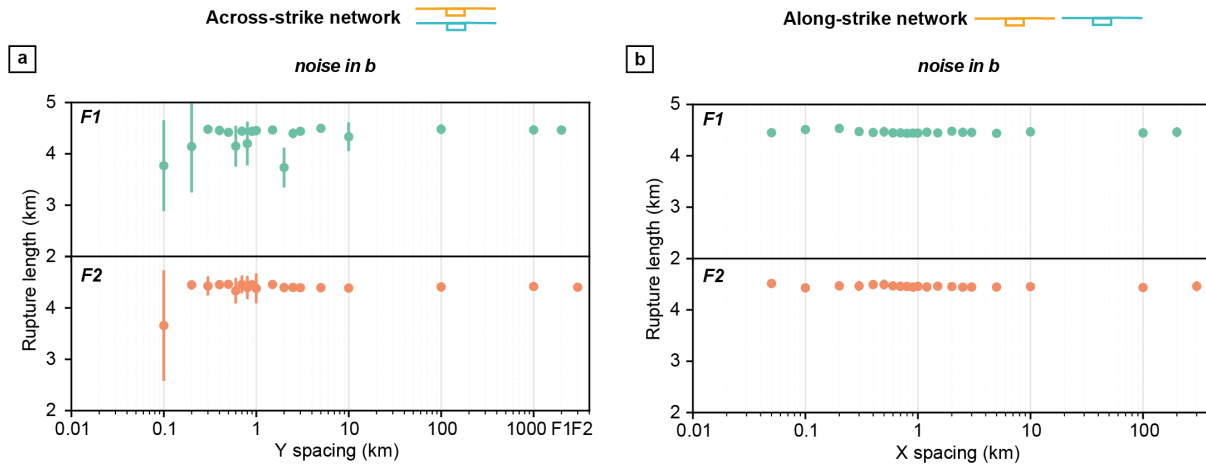
458   **Figure 10.** Variation of the rupture length (mean and standard deviation) with increasing separation for

459   the **(a)** across-strike and **(b)** along-strike network for individual faults.

460

461   To depict how decreasing fault spacing promotes greater complexity on the nucleation and

462   propagation of events, we investigate the variation of slip rate over time along a horizontal

463   cross-section at the middle of the fault for selected models (Figure 9). An isolated fault exhibits

464   a relatively straightforward seismic cycle, characterized by events initiating at the boundary

465   between velocity weakening and velocity strengthening material at the left of the fault,

466   followed by right-directed propagation and eventual full rupture of the locked patch (Figures

467   9a). The capability of single faults to generate partial ruptures depends on the W_s/L_∞ ratio. The

468   isolated fault modelled here has a W_s/L_∞ of 10.2, a value that exceeds the threshold estimated

469   in the 1D fault simulations by Cattania (2019), but that is smaller than the threshold identified

470   in the 2D models by Cattania & Segall (2019). Our results align with the findings of Cattania

471   & Segall (2019) indicating that partial-rupture emergence require a higher W_s/L_∞ in models

472   with greater dimensionality (e.g. by increasing the fault area, using more velocity-weakening

473   materials or reducing the characteristic distance). However, our results also show that partial

474   ruptures can occur in faults with smaller ratio than the one determined by Cattania and Segall

475   (2019) due to interaction with another fault across-strike.

476 Faults positioned 5 km apart across the strike of another fault exhibit distinct seismic behaviors

477 compared to isolated faults. While one of these faults maintains a seismic behavior similar to

478 the isolated fault (Figure 9c), the other fault displays events originating on either side of the

479 fault, yet still resulting in full and periodic ruptures (Figure 9b). As the across-strike spacing

480 decreases to 0.1 km, both faults exhibit increasingly complex seismic cycles, encompassing a

481 combination of full and partial ruptures originating from either side of the fault, bilateral

482 ruptures initiating at the fault's central region, as well as seismic ruptures with secondary

483 propagation fronts (Movie S1, Figure 9d-e). A few slow slip events are observed at the borders

484 of locked asperities in between full-rupture earthquakes (Movie S1). Regardless of the along-

485 or across-strike separations, faults do not rupture together, nor do we observe multievent

486 sequences in the same fault. A more general analysis of the variation of rupture lengths with

487 increasing across- and along-strike separation is depicted in Figure 10. While isolated faults

488 exhibit mean rupture lengths of ~4.5 km with small standard deviation (i.e. full ruptures), the

489 standard deviation of the rupture lengths increases (i.e. full and partial ruptures) with

490 decreasing across-strike distance (Figure 10a). Faults do not exhibit significant changes in

491 rupture length with decreasing along-strike distance, with events consistently rupturing the full

492 fault area (Figure 10b).

4. Discussion

494 Our study shows that the seismic cycle of faults within a small and simple fault network

495 depends on the fault network geometry and separation between faults, giving rise to distinct

496 patterns of rupture behavior, nucleation location, recurrence intervals and synchronicity

497 between faults.

498 Stress heterogeneities induced by fault interaction change the propagation style and nucleation

499 location of earthquakes (Figures 8-10). In across-strike faults with interaction, we additionally

500 observe more complex slip behaviors, such as slow slip events. The contrast between isolated

501 faults vs. faults arranged across-strike in terms of rupture extent and slip modes was also

502 observed by other numerical models of fault interaction (Romanet et al., 2018; Yin et al., 2023).

503 In their numerical experiment of two 1D faults, Romanet et al. (2018) found that, for a fault

504 spacing $\Delta y/L_\infty$ (0.51) and a/b ratio (0.5) equivalent to ours, faults generate earthquakes with

505 spatiotemporal complexities, but slow slip events only arise with a smaller L_f/L_∞ (0.5-1.5)

506 than that of our study ($L_f/L_\infty = 25$ or $W_f/L_\infty = 15.3$). Yin et al. (2023) also found that 2D

507   faults in *en-echelon* array can generate slow slip events with larger W_f/L_∞ (10.82-32.47) than

508   the one in Romanet et al.'s simulations. These observations suggest that slow slip behavior can

509   arise with either a larger fault size or a smaller nucleation length in 2D configurations compared

510   to 1D faults. This could be attributed to the absence of rupture arrest in the missing dimension

511   for the 1D faults, making them less likely to generate slow slip events when contrasted to 2D

512   faults (Li et al., 2022). Despite the observed trends, we do not identify other complex behaviors,

513   such as slip-bursts (i.e. full destabilization of the fault without rupture propagation, Romanet

514   et al., 2017) or multi-segments events (i.e., earthquakes propagating from one fault to the

515   other). The latter may be achieved with decreasing along-strike separation (Michel et al., 2024).

516   Different rupture extents and magnitude-frequency distributions in the fault system emerge due

517   to the spatial arrangement and the spacing between individual faults. The fact that partial

518   ruptures only occur with fault interaction and not in single faults, has been also observed in

519   strike-slip systems of 2 or 3 partially overlapping faults (Romanet et al., 2018; Yin et al., 2023).

520   Our study expands on these results by showing that partial ruptures do not occur when faults

521   are arranged along-strike. Although the simulated across-strike faults with reduced separation

522   are able to generate events with Mw smaller than the characteristic value of single faults, the

523   range of possible Mw is small compared to the Gutenberg-Richter distributions frequently

524   observed in instrumental, historical and paleoseismological records. Expanding the range of

525   modelled Mw values may involve incorporating greater geometrical complexities and frictional

526   heterogeneities into the system or by decreasing the characteristic distance Dc, which increases

527   the W/Linf ratio(Catannia, 2019).

528   While isolated faults show periodic cycles, periodicity changes as the separation between faults

529   varies. Far-apart faults (> 3 km) show periodic cycles (Figures 3c,d, 4a,c) and, at intermediate

530   across-strike distances, the recurrence times form either, unimodal or multimodal distributions

531   (0.4-3 km) and they transition into less periodic with small distances (<0.4 km). An even

532   greater variation of recurrence time could be achieved with a higher W_f/L_∞ ratio (Yin et al.,

533   2023). In contrast, the seismic cycle of normal faults remains periodic with decreasing along-

534   strike distance (Figure 3a-b). Overall, our results show that the coefficient of variation, a key

535   ingredient in PSHA models, is affected by the fault network geometry. This is currently not

536   considered in PSHA models globally (Gerstenberger et al., 2020). Therefore, this implies that

537   future PSHA models may wish to consider fault network geometry and the associated

538 interactions, especially for time-dependent models where earthquake triggering may be
539 considered.

540 The synchronization state of the combined seismic cycle of the faults varies in the presence of
541 fault interaction compared to the isolated case. Regardless of the different recurrence times of
542 isolated faults and the initial stress faults, the seismic cycle of across-strike faults that are close
543 together (<1.5 km) becomes more out-of-phase on average and with variable degree of
544 synchronization over time with decreasing distance. Along-strike faults that are close together
545 (<0.7 km) tend to be more synchronized with decreasing distance. The differences in
546 synchronicity within the seismic cycle of the fault system can be attributed to the static (or
547 Coulomb) stress changes occurring on a fault due to an earthquake on the neighboring fault.
548 The coseismic Coulomb Stress Transfer (CST) induced by an earthquake in a source fault to a
549 receiver fault is depicted in Figure 1b for a generic case where faults are initialized with equal
550 stress conditions and in Figure 11 for representative seismic events in selected simulations. The
551 static stress change due to a full-rupture event in the source fault is positive on the along-strike
552 direction (i.e., the receiver fault is stressed, Figure 1b; F2 in Figure 11d-e), while negative on
553 the across-strike direction (i.e., the receiver fault is relaxed; Figure 1c; F2 in Figure 11a-c). A
554 full-rupture event on a source fault located across-strike leads to a stress decrease in the receiver
555 fault and delays the occurrence of the next event on the receiver fault, contributing to the
556 desynchronization of the system (Figure 12). Full- and partial-rupture events also induce a
557 heterogeneous stress decrease on the receiver fault, promoting the development of partial
558 ruptures onto this fault where across-distance is small. These partial ruptures of variable rupture
559 length produce additional stress concentrations within the velocity-weakening region of the
560 receiver fault, which ultimately modifies the rupture propagation of subsequent events (Figure
561 11b). The combined interaction effects of clock-delay and heterogenous stress field contribute
562 to the less periodic behavior of the seismic cycle in faults where across-strike distance is small.
563 Conversely, an along-strike receiver fault would be positively stressed after an event on the
564 source fault (Figure 1b; F2 in Figure 11d-e), bringing the former closer to failure, and
565 ultimately leading to the synchronization of the system (Figure 8). The latter results are in line
566 with theoretical (Scholz, 2010) and historical and paleoseismological observations (Bell et al.,
567 2004), which suggest that synchronization is plausible between evenly-spaced along-strike
568 normal faults with similar slip rates, as observed in the extensional regions, such as Basin and
569 Range in Central Nevada. Additionally, the degree of synchronization and asynchronization in
570 along- and across-strike fault pairs respectively, intensifies as the separation decreases (Figure

571   10). The switch between more synchronized and less synchronized cycles occurs at a larger

572   across-strike spacing (~10 km) than along-strike (~3 km) spacing (Figure 4g,h). This is

573   consistent with the fact that the range of influence from a coseismic change on the stress-field

574   of a receiver fault that is across-strike varies with respect to a fault that is along-strike (3 cy et

575   al., 1987). Coulomb stresses decrease over a larger across-strike distance compared to the stress

576   increase over along-strike distances (Figure 1b-c). In the framework of PSHA, probabilistic

577   models of recurrence times could be refined by including this component of stress change

578   dependent of the fault network geometry.

579   Previous modelling work has studied fault interactions in strike-slip systems (Romanet et al.,

580   2018; Yin et al., 2023), whereas we focus on normal fault systems. A remaining question is to

581   what extent our results can be extrapolated to strike-slip systems. Although a quantitative

582   analysis of strike-slip fault networks is out of the scope of this study, we have shown in this

583   section that the effects on interaction in normal faults are qualitatively comparable to those in

584   strike-slip faults, with differences between the two fault types being smaller to those related to

585   model dimensions (3D vs. 2D simulations). We speculate that normal stress changes due to

586   free surface effects are not as impactful as those due to the network geometry except for shallow

587   depths. At such depths, two main differences with regards to the nucleation and propagation of

588   events could be highlighted. First, the decrease in normal stress due to the free surface condition

589   ahead of the rupture front, compared to the strike-slip case, brings the normal fault closer to

590   failure in this area, allowing the rupture front to jump ahead near the free surface (Oglesby et

591   al., 1998). Therefore, secondary propagation fronts such as those observed in some of our

592   simulations (e.g. Figure 8d) might be inhibited for the strike-slip case. Second, the free-surface

593   effect implies an increase in normal stress behind the rupture front in comparison to the strike-

594   slip case (Oglesby et al., 1998). This would make it more likely to nucleate shallow events in

595   strike-slip faults than in normal faults with the same initial conditions.

596   Finally, our study not only shows the critical role of fault separation in shaping the seismic

597   cycles of a fault system but also highlights the importance of the fault-network geometry in

598   modulating changes in stress-loading history of individual faults. The latter aspect was

599   previously noted by Sgambato et al. (2020) in the southern Apennines by means of Coulomb

600   stress transfer modelling. We show that static-stress delay resulting from interaction between

601   across-strike faults have a larger effect on the earthquake cycle than static-stress triggering

602   between along strike-faults. While the topic of earthquake clustering and clock-advance of

603 seismic events in highly stressed areas have received considerable attention, there has been
604 relatively less focus on event delays occurring within faults subjected to stress shadows (Harris
605 & Simpson, 1996, 1998). This imbalance is partly due to the inherent challenges behind
606 proving that delayed events are indeed related to stress shadows, compared to well-documented
607 triggering events in highly stressed regions (Freed, 2012; Kroll et al., 2017). However, previous
608 work has highlighted the role of stress shadows on decennial (Harris & Simpson, 1996, 1998;
609 Kroll et al., 2017; Toda et al., 2012) and millennial timescales (Sgambato et al., 2020;
610 Wedmore et al., 2017). In this context, our research provides evidence that the influence of
611 stress shadows may be even more significant than stress increases on varying timescales. These
612 aspects should be included in future time-dependent statistical models used in probabilistic
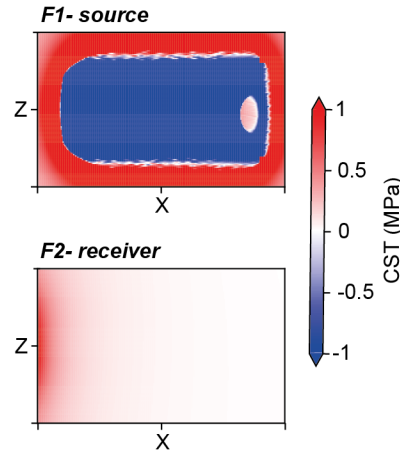613 hazard assessment.

614

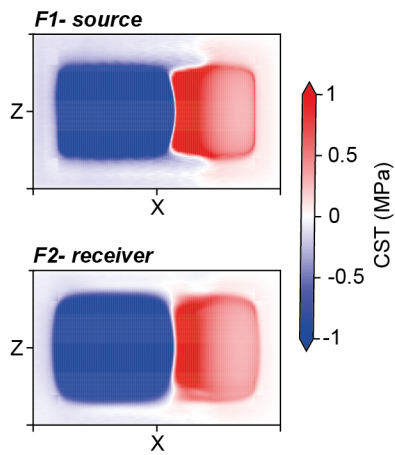**Across-strike spacing = 0.1 km (noise in b)**

a *Full rupture | t = 377.04 yr*
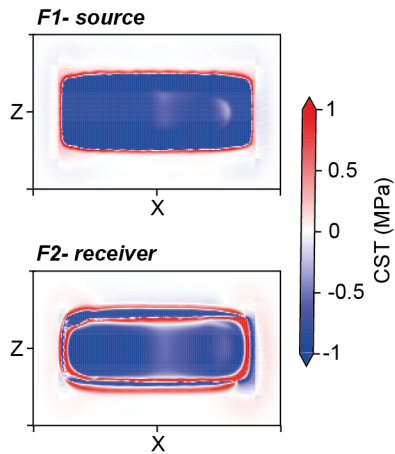
Along-strike spacing = 0.05 km (noise in b)

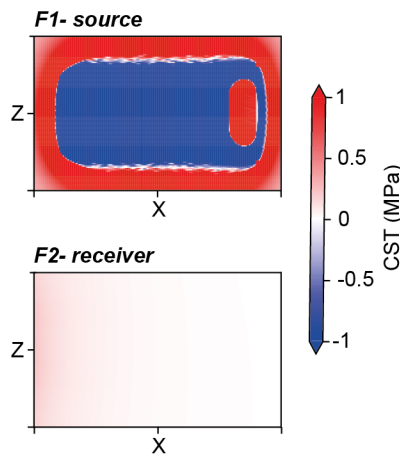d *Full rupture | t = 322.31 yr*

b *Partial rupture | t = 266.04 yr*

Along-strike spacing = 0.5 km (noise in b)

e *Full rupture in F1 | t =305.87 yr*

Across-strike spacing = 0.5 km (noise in b)

c *Full rupture | t = 491.35 yr*
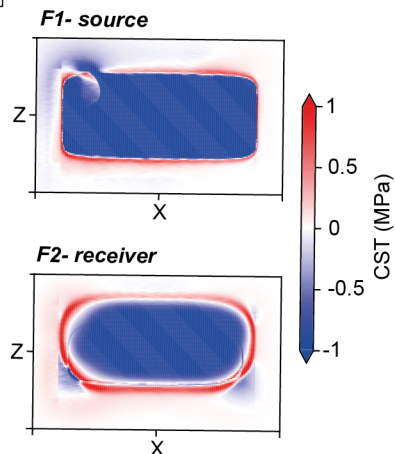
615

616 **Figure 11:** Coseismic Coulomb stress transfer (CST) for representative events for across-strike

617 spacings of **(a-b)** 0.1 km, **(c)** 0.5 km and along-strike spacings of **(d)** 0.05 km and **(e)** 0.5 km (see Text

618 S2 for derivation). The coseismic phase is considered as the time interval in which at least one element

slips at a higher rate than 0.01 m/s. The CST introduced by an event in a neighboring fault is negative for across-strike faults and positive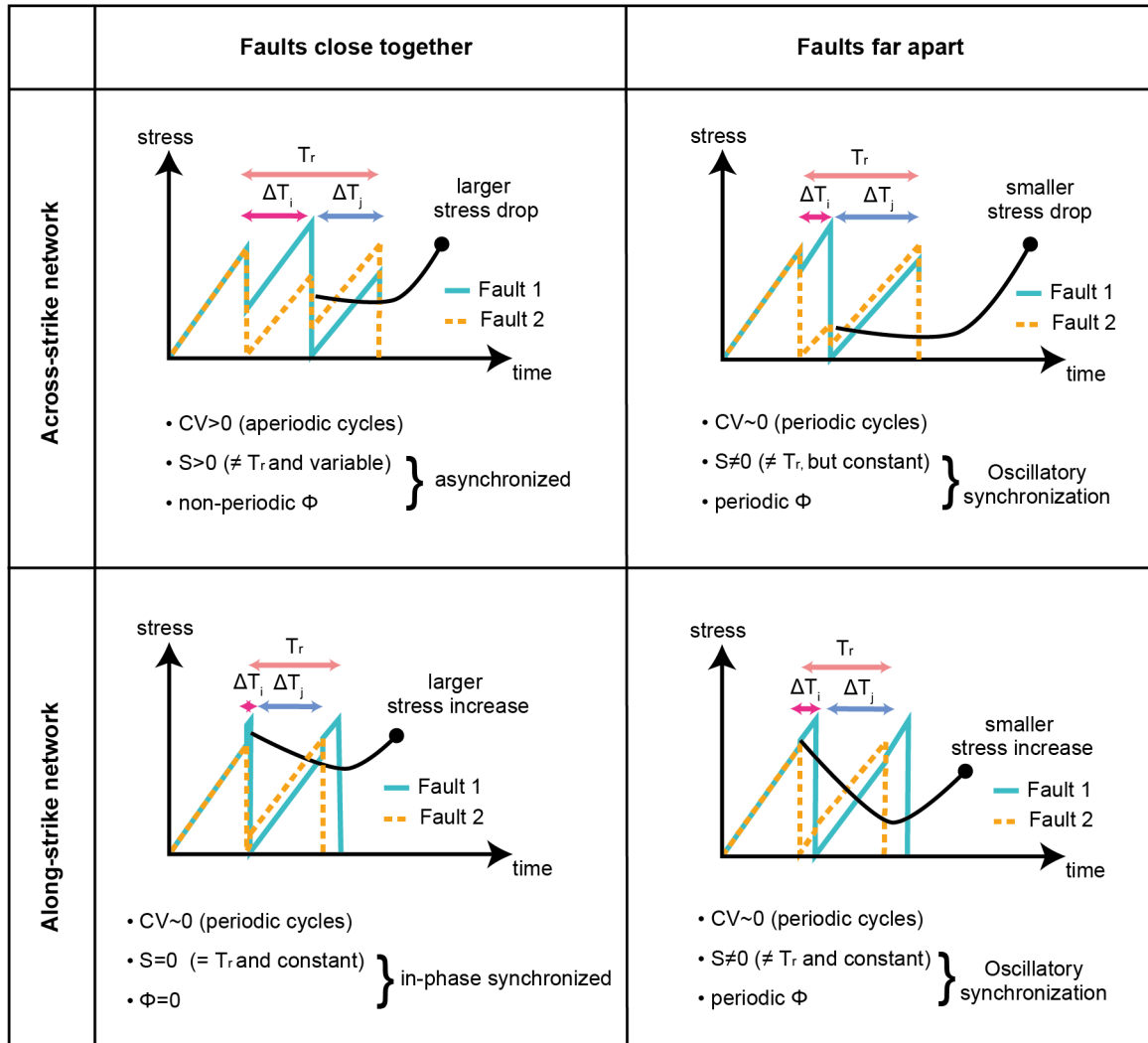 for along-strike faults. For the same fault separation, the magnitude of CST is smaller for the along-strike network than for the across-strike network. The color-scale has been adjusted between -1MPa and 1MPa to better visualize the small CST of faults separated by an along-strike distance of 0.5 km.

Figure 12. Schematic diagrams showing the effect of the fault network geometry and spacing on the earthquake cycle's periodicity (depicted by CV) and synchronicity (S) of each fault

5. Conclusions

We conducted numerical simulations of the earthquake cycle of two normal faults to explore the effect of a simple fault network geometry and spacing between faults in their combined

seismic cycle. Our findings illustrate that far-apart across-strike faults (> 3 km) behave as single isolated faults showing periodic cycles; they show either periodic or less periodic behavior with intermediate distances (0.4-3 km) but become less periodic when close together (<0.4 km). Faults show cycles with varying degrees of synchronization when the across-strike spacing is small (< 0.2 km). Moreover, while single faults produce full ruptures with a characteristic magnitude, reducing the across-strike spacing leads to more complex sequences with variability of the hypocenter location and emergence of partial ruptures, which ultimately gives rise to a wider range of magnitudes.

Unlike faults situated across-strike, the cycle periodicity and characteristic behavior of faults situated along-strike remains unaffected irrespective of their spacing. However, closely spaced faults situated along-strike (≤0.9 km) tend to display similar recurrence times and to evolve towards a state of persistent synchronization, with their combined seismic cycles becoming increasingly in phase as their separation decreases. Moreover, there is less variability of the nucleation location compared to the across-strike case. Altogether, we show that across-strike distance between faults has a larger effect on recurrence time, synchronicity, nucleation location, extent, and propagation of the seismic rupture than along-strike distance. We suggest that fault network geometry and the effects on key earthquake occurrence parameters (e.g. CV, mean recurrence time) should be considered when undertaking seismic hazard assessment.

Acknowledgements

Open Research

The input files to reproduce the results of this work are available at the following link (add link zenodo) (Rodriguez Piceda et al., 202x).

Code availability: QDYN is open source (Luo et al. 2017). The simulations were run with the QDYN version release 3.0.0.

References

Abe, Y., & Kato, N. (2013). Complex Earthquake Cycle Simulations Using a Two-Degree-of-Freedom Spring-Block Model with a Rate- and State-Friction Law. *Pure and Applied Geophysics*, *170*(5), 745–765. https://doi.org/10.1007/s00024-011-0450-8

Barbot, S. (2019). Slow-slip, slow earthquakes, period-two cycles, full and partial ruptures, and deterministic chaos in a single asperity fault. *Tectonophysics*, *768*, 228171. https://doi.org/10.1016/j.tecto.2019.228171

Barbot, S. (2021). A Spectral Boundary-Integral Method for Quasi-Dynamic Ruptures of Multiple Parallel Faults. *Bulletin of the Seismological Society of America*, *111*(3), 1614–1630. https://doi.org/10.1785/0120210004

Bell, J. W., Caskey, S. J., Ramelli, A. R., & Guerrieri, L. (2004). Pattern and Rates of Faulting in the Central Nevada Seismic Belt, and Paleoseismic Evidence for Prior Beltlike Behavior. *Bulletin of the Seismological Society of America*, *94*(4), 1229–1254. https://doi.org/10.1785/012003226

Benedetti, L., Manighetti, I., Gaudemer, Y., Finkel, R., Malavieille, J., Pou, K., et al. (2013). Earthquake synchrony and clustering on Fucino faults (Central Italy) as revealed from

676   in situ 36Cl exposure dating. *Journal of Geophysical Research: Solid Earth*, *118*(9),

677   4948–4974. https://doi.org/10.1002/jgrb.50299

678 Biemiller, J., & Lavier, L. (2017). Earthquake supercycles as part of a spectrum of normal fault

679   slip styles. *Journal of Geophysical Research: Solid Earth*, *122*(4), 3221–3240.

680   https://doi.org/10.1002/2016JB013666

681 Boschi, E., Gasperini, P., & Mulargia, F. (1995). Forecasting where larger crustal earthquakes

682   are likely to occur in Italy in the near future. *Bulletin of the Seismological Society of*

683   *America*, *85*(5), 1475–1482. https://doi.org/10.1785/BSSA0850051475

684 Cattania, C. (2019). Complex Earthquake Sequences On Simple Faults. *Geophysical Research*

685   *Letters*, *46*(17–18), 10384–10393. https://doi.org/10.1029/2019GL083628

686 Cattania, C., & Segall, P. (2019). Crack Models of Repeating Earthquakes Predict Observed

687   Moment-Recurrence Scaling. *Journal of Geophysical Research: Solid Earth*, *124*(1),

688   476–503. https://doi.org/10.1029/2018JB016056

689 Cinti, F. R., Pantosti, D., Lombardi, A. M., & Civico, R. (2021). Modeling of earthquake

690   chronology from paleoseismic data: Insights for regional earthquake recurrence and

691   earthquake storms in the Central Apennines. *Tectonophysics*, *816*, 229016.

692   https://doi.org/10.1016/j.tecto.2021.229016

693 Corbi, F., Funiciello, F., Brizzi, S., Lallemand, S., & Rosenau, M. (2017). Control of asperities

694   size and spacing on seismic behavior of subduction megathrusts. *Geophysical Research*

695   *Letters*, *44*(16), 8227–8235. https://doi.org/10.1002/2017GL074182

696 Cornell, C. A. (1968). Engineering seismic risk analysis. *Bulletin of the Seismological Society*

697   *of America*, *58*(5), 1583–1606. https://doi.org/10.1785/BSSA0580051583

698   Cowie, P. A., Roberts, G. P., Bull, J. M., & Visini, F. (2012). Relationships between fault

699   geometry, slip rate variability and earthquake recurrence in extensional settings.

700   *Geophysical Journal International*, *189*(1), 143–160. https://doi.org/10.1111/j.1365-

701   246X.2012.05378.x

702   Cowie, P. A., Scholz, C. H., Roberts, G. P., Faure Walker, J. P., & Steer, P. (2013). Viscous

703   roots of active seismogenic faults revealed by geologic slip rate variations. *Nature*

704   *Geoscience*, *6.12*(November), 1036–1040. https://doi.org/10.1038/ngeo1991

705   Day, S. M., Dalguer, L. A., Lapusta, N., & Liu, Y. (2005). Comparison of finite difference and

706   boundary integral solutions to three-dimensional spontaneous rupture. *Journal of*

707   *Geophysical Research: Solid Earth*, *110*(B12). https://doi.org/10.1029/2005JB003813

708   Dieterich, James H., & Richards-Dinger, K. B. (2010). Earthquake Recurrence in Simulated

709   Fault Systems. *Pure and Applied Geophysics*, *167*(8), 1087–1104.

710   https://doi.org/10.1007/s00024-010-0094-0

711   Dieterich, J.H. (1979). Modeling of rock friction 1. Experimental results and constitutive

712   equations. *Journal of Geophysical Research: Solid Earth*, *84*(B5), 2161–2168.

713   https://doi.org/10.1029/JB084iB05p02161

714   Ellsworth, W. L. (1995). - Characteristic earthquakes and long-term earthquake forecasts:

715   Implications of central california seismicity. In F. Y. Cheng & M.-S. Sheu (Eds.),

716   *Urban Disaster Mitigation: The Role of Engineering and Technology* (pp. 1–14).

717   Oxford: Pergamon. https://doi.org/10.1016/B978-008041920-6/50007-5

718   Field, E. H., Milner, K. R., Hardebeck, J. L., Page, M. T., van der Elst, N., Jordan, T. H., et al.

719   (2017). A Spatiotemporal Clustering Model for the Third Uniform California

720   Earthquake Rupture Forecast (UCERF3-ETAS): Toward an Operational Earthquake

721   Forecast. *Bulletin of the Seismological Society of America*, *107*(3), 1049–1081.

722   https://doi.org/10.1785/0120160173

723 Freed, A. M. (2012). Casting stress shadows. *Nature Geoscience*, *5*(6), 371–372.

724   https://doi.org/10.1038/ngeo1489

725 Frohlich, C., & Davis, S. D. (1990). Single-Link Cluster Analysis as a Method to Evaluate

726   Spatial and Temporal Properties of Earthquake Catalogues. *Geophysical Journal*

727   *International*, *100*(1), 19–32. https://doi.org/10.1111/j.1365-246X.1990.tb04564.x

728 Fujiwara, H., Kawai, S., Aoi, S., Ishii, T., Okumura, T., Hayakawa, Y., et al. (2006). Japan

729   seismic hazard information station, J-SHIS. In *Proceedings of the 8th US National*

730   *Conference on Earthquake Engineering* (Vol. 274).

731 Gerstenberger, M. C., Marzocchi, W., Allen, T., Pagani, M., Adams, J., Danciu, L., et al.

732   (2020). Probabilistic Seismic Hazard Analysis at Regional and National Scales: State

733   of the Art and Future Challenges. *Reviews of Geophysics*, *58*(2).

734   https://doi.org/10.1029/2019RG000653

735 Goldfinger, C., Nelson, C. H., Morey, A. E., Johnson, J. E., Patton, J. R., Karabanov, E. B., et

736   al. (2012). *Turbidite event history—Methods and implications for Holocene*

737   *paleoseismicity of the Cascadia subduction zone* (No. 1661- F). *Professional Paper*.

738   U.S. Geological Survey. https://doi.org/10.3133/pp1661F

739 Goodall, H. J., Gregory, L. C., Wedmore, L. N. J., McCaffrey, K. J. W., Amey, R. M. J.,

740   Roberts, G. P., et al. (2021). Determining Histories of Slip on Normal Faults With

741   Bedrock Scarps Using Cosmogenic Nuclide Exposure Data. *Tectonics*, *40*(3),

742   e2020TC006457. https://doi.org/10.1029/2020TC006457

743 Gu, Y., & Wong, T.-F. (1994). Nonlinear Dynamics of the Transition from Stable Sliding to

744 Cyclic Stick-Slip in Rock. In *Nonlinear Dynamics and Predictability of Geophysical*

745 *Phenomena* (pp. 15–35). American Geophysical Union (AGU).

746 https://doi.org/10.1029/GM083p0015

747 Harris, R. A., & Simpson, R. W. (1996). In the shadow of 1857-the effect of the great Ft. Tejon

748 earthquake on subsequent earthquakes in southern California. *Geophysical Research*

749 *Letters*, *23*(3), 229–232. https://doi.org/10.1029/96GL00015

750 Harris, R. A., & Simpson, R. W. (1998). Suppression of large earthquakes by stress shadows:

751 A comparison of Coulomb and rate-and-state failure. *Journal of Geophysical Research:*

752 *Solid Earth*, *103*(B10), 24439–24451. https://doi.org/10.1029/98JB00793

753 He, C. (2003). Interaction between two sliders in a system with rate- and state-dependent

754 friction. *Science in China Series D: Earth Sciences*, *46*(2), 67–74.

755 https://doi.org/10.1360/03dz0006

756 Hillers, G., Mai, P. M., Ben-Zion, Y., & Ampuero, J.-P. (2007). Statistical properties of

757 seismicity of fault zones at different evolutionary stages. *Geophysical Journal*

758 *International*, *169*(2), 515–533. https://doi.org/10.1111/j.1365-246X.2006.03275.x

759 Iezzi, F., Roberts, G., Faure Walker, J., Papanikolaou, I., Ganas, A., Deligiannakis, G., et al.

760 (2021). Temporal and spatial earthquake clustering revealed through comparison of

761 millennial strain-rates from 36Cl cosmogenic exposure dating and decadal GPS strain-

762 rate. *Scientific Reports*, *11*(1), 23320. https://doi.org/10.1038/s41598-021-02131-3

763 Kagan, Y. Y., & Jackson, D. D. (1991). Long-term earthquake clustering. *Geophysical Journal*

764 *International*, *104*(1), 117–133. https://doi.org/10.1111/j.1365-246X.1991.tb02498.x

765 Kagan, Y. Y., Jackson, D. D., & Geller, R. J. (2012). Characteristic Earthquake Model, 1884–

766   2011, R.I.P. *Seismological Research Letters*, *83*(6), 951–953.

767   https://doi.org/10.1785/0220120107

768 Kaneko, Y., Avouac, J.-P., & Lapusta, N. (2010). Towards inferring earthquake patterns from

769   geodetic observations of interseismic coupling. *Nature Geoscience*, *3*(5), 363–369.

770   https://doi.org/10.1038/ngeo843

771 Kroll, K. A., Richards-Dinger, K. B., Dieterich, J. H., & Cochran, E. S. (2017). Delayed

772   Seismicity Rate Changes Controlled by Static Stress Transfer. *Journal of Geophysical*

773   *Research: Solid Earth*, *122*(10), 7951–7965. https://doi.org/10.1002/2017JB014227

774 Lapusta, N., Rice, J. R., Ben-Zion, Y., & Zheng, G. (2000). Elastodynamic analysis for slow

775   tectonic loading with spontaneous rupture episodes on faults with rate- and state-

776   dependent friction. *Journal of Geophysical Research: Solid Earth*, *105*(B10), 23765–

777   23789. https://doi.org/10.1029/2000JB900250

778 Li, M., Pranger, C., & van Dinther, Y. (2022). Characteristics of Earthquake Cycles: A Cross-

779   Dimensional Comparison of 0D to 3D Numerical Models. *Journal of Geophysical*

780   *Research: Solid Earth*, *127*(8), e2021JB023726.

781   https://doi.org/10.1029/2021JB023726

782 Luo, Y., & Ampuero, J.-P. (2018). Stability of faults with heterogeneous friction properties

783   and effective normal stress. *Tectonophysics*, *733*, 257–272.

784   https://doi.org/10.1016/j.tecto.2017.11.006

785 Luo, Y., Ampuero, J. P., Galvez, P., Ende, M. van den, & Idini, B. (2017, February). QDYN:

786   a Quasi-DYNamic earthquake simulator (v1.1) (Version qdyn_1.1). Zenodo.

787   https://doi.org/10.5281/zenodo.322459

788   Marco, S., Stein, M., Agnon, A., & Ron, H. (1996). Long-term earthquake clustering: A

789   50,000-year paleoseismic record in the Dead Sea Graben. *Journal of Geophysical*

790   *Research: Solid Earth*, *101*(B3), 6179–6191. https://doi.org/10.1029/95JB01587

791   Marone, C. (1998). Laboratory-Derived Friction Laws and Their Application to Seismic

792   Faulting. *Annual Review of Earth and Planetary Sciences*, *26*(1), 643–696.

793   https://doi.org/10.1146/annurev.earth.26.1.643

794   Marzocchi, W., Selva, J., Cinti, F. R., Montone, P., Pierdominici, S., Schivardi, R., & Boschi,

795   E. (2009). On the occurrence of large earthquakes: New insights from a model based

796   on interacting faults embedded in a realistic tectonic setting. *Journal of Geophysical*

797   *Research: Solid Earth*, *114*(B1). https://doi.org/10.1029/2008JB005822

798   McCalpin, J. P., & Nishenko, S. P. (1996). Holocene paleoseismicity, temporal clustering, and

799   probabilities of future large (M > 7) earthquakes on the Wasatch fault zone, Utah.

800   *Journal of Geophysical Research: Solid Earth*, *101*(B3), 6233–6253.

801   https://doi.org/10.1029/95JB02851

802   Michel, S., Scotti, O., Hok, S., Bhat, H., Khairdast, N., Almakari, M., & Cheng, J. (2024, March

803   11). Evaluating probabilities of earthquake fault jumps from 2D numerical simulation

804   of seismic cycles. https://doi.org/10.5194/egusphere-egu24-18480

805   Mildon, Z. K., Roberts, G. P., Faure Walker, J. P., & Iezzi, F. (2017). Coulomb stress transfer

806   and fault interaction over millennia on non-planar active normal faults: the Mw 6.5–5.0

807   seismic sequence of 2016–2017, central Italy. *Geophysical Journal International*,

808   *210*(2), 1206–1218. https://doi.org/10.1093/gji/ggx213

809   Mildon, Z. K., Roberts, G. P., Faure Walker, J. P., & Toda, S. (2019). Coulomb pre-stress and

810   fault bends are ignored yet vital factors for earthquake triggering and hazard. *Nature*

811   *Communications*, *10*(1), 2744. https://doi.org/10.1038/s41467-019-10520-6

812   Mildon, Z. K., Roberts, G. P., Faure Walker, J. P., Beck, J., Papanikolaou, I., Michetti, A. M.,

813   et al. (2022). Surface faulting earthquake clustering controlled by fault and shear-zone

814   interactions. *Nature Communications*, *13*(1), 7126. https://doi.org/10.1038/s41467-

815   022-34821-5

816   Molina-Ormazabal, D., Ampuero, J.-P., & Tassara, A. (2023). Diverse slip behaviour of

817   velocity-weakening fault barriers. *Nature Geoscience*, *16*(12), 1200–1207.

818   https://doi.org/10.1038/s41561-023-01312-1

819   Moore, D. E., & Rymer, M. J. (2007). Talc-bearing serpentinite and the creeping section of the

820   San Andreas fault. *Nature*, *448*(7155), 795–797. https://doi.org/10.1038/nature06064

821   Mulargia, F., Stark, P. B., & Geller, R. J. (2017). Why is Probabilistic Seismic Hazard Analysis

822   (PSHA) still used? *Physics of the Earth and Planetary Interiors*, *264*, 63–75.

823   https://doi.org/10.1016/j.pepi.2016.12.002

824   Nicol, A., Van Dissen, R. J., Stirling, M. W., & Gerstenberger, M. C. (2016). Completeness of

825   the Paleoseismic Active-Fault Record in New Zealand. *Seismological Research Letters*,

826   *87*(6), 1299–1310. https://doi.org/10.1785/0220160088

827   Oglesby, D. D., Archuleta, R. J., & Nielsen, S. B. (1998). Earthquakes on Dipping Faults: The

828   Effects of Broken Symmetry. *Science*, *280*(5366), 1055–1059.

829   https://doi.org/10.1126/science.280.5366.1055

830   Okada, Y. (1992). Internal deformation due to shear and tensile faults in a half-space. *Bulletin*

831   *of   the   Seismological   Society   of   America*,   *82*(2),   1018–1040.

832   https://doi.org/10.1785/BSSA0820021018

833   Perlin, K. (1985). An image synthesizer. *ACM SIGGRAPH Computer Graphics*, *19*(3), 287–

834   296. https://doi.org/10.1145/325165.325247

835   Reasenberg, P. (1985). Second-order moment of central California seismicity, 1969–1982.

836   *Journal   of   Geophysical   Research: Solid   Earth*,   *90*(B7),   5479–5495.

837   https://doi.org/10.1029/JB090iB07p05479

838   Rice, J. R. (1993). Spatio-temporal complexity of slip on a fault. *Journal of Geophysical*

839   *Research: Solid Earth*, *98*(B6), 9885–9907. https://doi.org/10.1029/93JB00191

840   Robinson, R., & Benites, R. (1995). Synthetic seismicity models of multiple interacting faults.

841   *Journal   of   Geophysical   Research: Solid   Earth*,   *100*(B9),   18229–18238.

842   https://doi.org/10.1029/95JB01569

843   Romanet, P., Bhat, H. S., Jolivet, R., & Madariaga, R. (2018). Fast and Slow Slip Events

844   Emerge Due to Fault Geometrical Complexity. *Geophysical Research Letters*, *45*(10),

845   4809–4819. https://doi.org/10.1029/2018GL077579

846   Rubin, A. M. (2008). Episodic slow slip events and rate-and-state friction. *Journal of*

847   *Geophysical Research: Solid Earth*, *113*(B11). https://doi.org/10.1029/2008JB005642

848   Rubin, A. M., & Ampuero, J.-P. (2005). Earthquake nucleation on (aging) rate and state faults.

849   *Journal   of   Geophysical   Research: Solid   Earth*,   *110*(B11).

850   https://doi.org/10.1029/2005JB003686

851 Ruina, A. (1983). Slip instability and state variable friction laws. *Journal of Geophysical*
852   *Research*, *88*(B12), 10359–10370. https://doi.org/10.1029/JB088iB12p10359

853 Scholz, C. H. (2010). Large Earthquake Triggering, Clustering, and the Synchronization of
854   Faults. *Bulletin of the Seismological Society of America*, *100*(3), 901–909.
855   https://doi.org/10.1785/0120090309

856 Sgambato, C., Faure Walker, J. P., Mildon, Z. K., & Roberts, G. P. (2020). Stress loading
857   history of earthquake faults influenced by fault/shear zone geometry and Coulomb pre-
858   stress. *Scientific Reports*, *10*(1), 12724. https://doi.org/10.1038/s41598-020-69681-w

859 Sgambato, C., Faure Walker, J. P., Roberts, G. P., Mildon, Z. K., & Meschis, M. (2023).
860   Influence of Fault System Geometry and Slip Rates on the Relative Role of Coseismic
861   and Interseismic Stresses on Earthquake Triggering and Recurrence Variability.
862   *Journal of Geophysical Research: Solid Earth*, *128*(11), e2023JB026496.
863   https://doi.org/10.1029/2023JB026496

864 Shi, P., Wei, M., & Barbot, S. (2022). Contribution of Viscoelastic Stress to the
865   Synchronization of Earthquake Cycles on Oceanic Transform Faults. *Journal of*
866   *Geophysical Research: Solid Earth*, *127*(8), e2022JB024069.
867   https://doi.org/10.1029/2022JB024069

868 Spagnuolo, E., Herrero, A., & Cultrera, G. (2012). The effect of directivity in a PSHA
869   framework. *Geophysical Journal International*, *191*(2), 616–626.
870   https://doi.org/10.1111/j.1365-246X.2012.05630.x

871 Stirling, M., McVerry, G., Gerstenberger, M., Litchfield, N., Van Dissen, R., Berryman, K., et
872   al. (2012). National Seismic Hazard Model for New Zealand: 2010 Update. *Bulletin of*

873   *the Seismological Society of America*, *102*(4), 1514–1542.

874   https://doi.org/10.1785/0120110170

875   Thompson, E. M., & Worden, C. B. (2017). Estimating Rupture Distances without a Rupture.

876   *Bulletin of the Seismological Society of America*, *108*(1), 371–379.

877   https://doi.org/10.1785/0120170174

878   Toda, S., Stein, R. S., Beroza, G. C., & Marsan, D. (2012). Aftershocks halted by static stress

879   shadows. *Nature Geoscience*, *5*(6), 410–413. https://doi.org/10.1038/ngeo1465

880   Ward, S. N. (2000). San Francisco Bay Area Earthquake Simulations: A Step Toward a

881   Standard Physical Earthquake Model. *Bulletin of the Seismological Society of America*,

882   *90*(2), 370–386. https://doi.org/10.1785/0119990026

883   Wedmore, L. N. J., Faure Walker, J. P., Roberts, G. P., Sammonds, P. R., McCaffrey, K. J. W.,

884   & Cowie, P. A. (2017). A 667 year record of coseismic and interseismic Coulomb stress

885   changes in central Italy reveals the role of fault interaction in controlling irregular

886   earthquake recurrence intervals. *Journal of Geophysical Research: Solid Earth*, *122*(7),

887   5691–5711. https://doi.org/10.1002/2017JB014054

888   Wei, M., & Shi, P. (2021). Synchronization of Earthquake Cycles of Adjacent Segments on

889   Oceanic Transform Faults Revealed by Numerical Simulation in the Framework of

890   Rate-and-State Friction. *Journal of Geophysical Research: Solid Earth*, *126*(1),

891   e2020JB020231. https://doi.org/10.1029/2020JB020231

892   Wells, D. L., & Coppersmith, K. J. (1994). New empirical relationships among magnitude,

893   rupture length, rupture width, rupture area, and surface displacement. *Bulletin of the*

894   *Seismological Society of America*, *84*(4), 974–1002.

895   https://doi.org/10.1785/BSSA0840040974

896   Yin, Y., Galvez, P., Heimisson, E. R., & Wiemer, S. (2023). The role of three-dimensional

897   fault interactions in creating complex seismic sequences. *Earth and Planetary Science*

898   *Letters*, *606*, 118056. https://doi.org/10.1016/j.epsl.2023.118056

899   Yoshida, S., & Kato, N. (2003). Episodic aseismic slip in a two-degree-of-freedom block-

900   spring   model.   *Geophysical   Research   Letters*,   *30*(13).

901   https://doi.org/10.1029/2003GL017439

902   Zöller, G., & Hainzl, S. (2007). Recurrence Time Distributions of Large Earthquakes in a

903   Stochastic Model for Coupled Fault Systems: The Role of Fault Interaction. *Bulletin*

904   *of   the   Seismological   Society   of   America*,   *97*(5),   1679–1687.

905   https://doi.org/10.1785/0120060262

906

Supporting Information for

Normal fault interactions in seismic cycles and the impact of fault network geometry

Constanza Rodriguez Piceda*(1), Zoë K. Mildon(1), Martijn van den Ende(2), Jean-Paul Ampuero(2), Billy Andrews(1)

(1)   University of Plymouth, School of Geography, Earth and Environmental Sciences, Plymouth, United Kingdom
(2)   Université Côte d'Azur, Observatoire de la Côte d'Azur, IRD, CNRS, Géoazur, Nice, France

* Corresponding author: Constanza Rodriguez Piceda
(constanza.rodriguezpiceda@plymouth.ac.uk)

Contents of this file

Supplementary Text S1 to S2

Figures S1

Additional Supporting Information (Files uploaded separately)

Movie S1: Upper panel shows the evolution of the slip rate over time of one fault for model group 'noise in b'. Lower panel shows the time-series of the maximum slip rate for that fault.

Movie S2: Upper panel shows the evolution of the slip rate over time of two faults separated by an across-strike distance of 0.1 km for model group 'noise in b'. Lower panel shows the time-series of the maximum slip rate for those faults.

Movie S3: Upper panel shows the evolution of the slip rate over time of two faults separated by an across-strike distance of 5 km for model group 'noise in b'. Lower panel shows the time-series of the maximum slip rate for those faults.

Movie S4: Upper panel shows the evolution of the slip rate over time of two faults separated by an along-strike distance of 0.1 km for model group 'noise in b'. Lower panel shows the time-series of the maximum slip rate for those faults.

Movie S5: Upper panel shows the evolution of the slip rate over time of two faults separated by an along-strike distance of 5 km for model group 'noise in b'. Lower panel shows the time-series of the maximum slip rate for those faults.

Introduction

This file includes: the description of the calculation of the initial normal stress in the simulations (**Supplementary text S1**); a figure with the time evolution of the synchronicity (**Figure S1**) and a description of the calculation of the coseismic coulomb stress transfer for selected events of the simulations (**Supplementary text S2**).

Text S1. Calculation of initial normal stress

Lapusta et al. (2000) proposes that the variation of effective normal stress with depth in a strike-slip fault is as following: effective normal stress is equal to the lithostatic pressure minus the hydrostatic pore pressure at shallow depth (up to 2.6 km), with a transition to lithostatatic pore pressure gradient with a 50 MPa offset at depth (z):

$$\bar{\sigma}_l = min \begin{cases} 50\ Mpa \\ 2.8 + 18 * z/km \end{cases}$$

We account for the dip angle of the normal fault (α) in our simulation:

$$\bar{\sigma} = \bar{\sigma}_l * sin\alpha$$
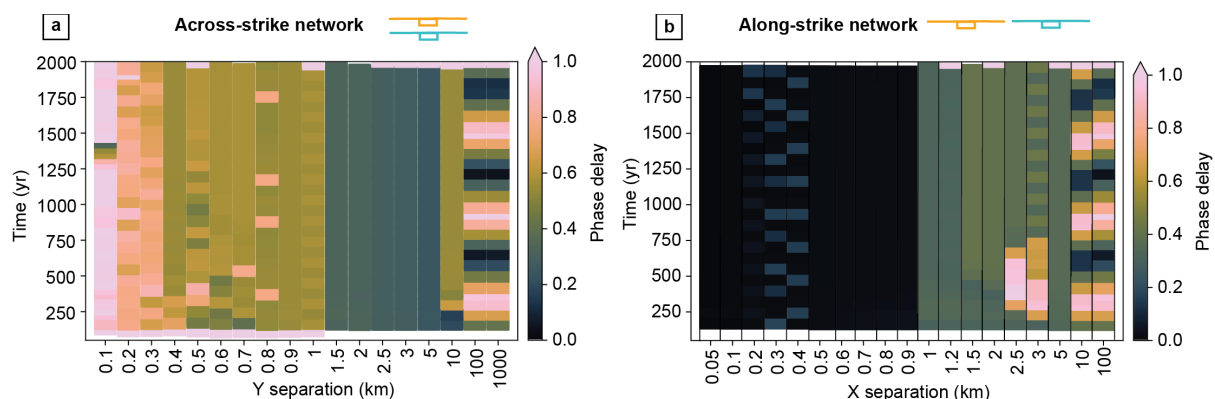
Figure S1: Time evolution of phase delay as a function of the (a) across-strike and (b) along-strike spacing between faults.

Text S2. Calculation of Coulomb stress-transfer

The coseismic coulomb stress transfer (ΔC) can be calculated as (King et al., 1994):

$$\Delta C = \Delta\tau + f^*\Delta\sigma$$

Where $\Delta\tau$ is the shear stress-change, $\Delta\sigma$ is the normal stress change before and after the earthquake and f^* the friction coefficient.